THE SUPERPOSITION OF DIFFUSION MODELS

Anonymous authors
Paper under double-blind review

ABSTRACT

The Cambrian explosion of easily accessible pre-trained diffusion models suggests a demand for methods that combine multiple different pre-trained diffusion models without incurring the significant computational burden of re-training a larger combined model. In this paper, we cast the problem of combining multiple pre-trained diffusion models at the generation stage under a novel proposed framework termed superposition. Theoretically, we derive superposition from rigorous first principles stemming from the celebrated continuity equation and design two novel algorithms tailor-made for combining diffusion models in SUPERDIFF. We demonstrate that SUPERDIFF is scalable to large pre-trained diffusion models as superposition is performed *solely through composition during inference*, and also enjoys painless implementation as it combines different pre-trained vector fields through an automated re-weighting scheme. Notably, we show that SUPERDIFF is efficient during inference time, and mimics traditional composition operators such as the logical OR and the logical AND. We empirically demonstrate the utility of using SUPERDIFF for generating more diverse images on CIFAR-10, more faithful prompt conditioned image editing using Stable Diffusion, and improved unconditional *de novo* structure design of proteins.

Figure 1: Concept interpolations via different methods: SUPERDIFF (top row), the averaging of outputs with different prompts (middle row), and joint prompting with standard Stable Diffusion (SD) (bottom row) for six different prompt combinations. Here we use SUPERDIFF with the AND operation (sampling equal densities).

1 INTRODUCTION

The design and application of generative models at scale are arguably one of the fastest-growing use cases of machine learning, with generational leaps in performance that often exceed expert expectations (Steinhardt, 2022). A few of the central facilitators of this rapid progress are the availability of high-quality training data and large computing hardware (Kaplan et al., 2020); which in tandem provide a tried and trusted recipe to scale generative models in a variety of data modalities such as video generation (Brooks et al., 2024), natural language understanding (OpenAI, 2023; Achiam

et al., 2023; Dong et al., 2022), and other challenging domains like mathematical reasoning (Trinh et al., 2024), or code assistance (Bubeck et al., 2023). As a result, it is not surprising that a driving force behind current generative modeling research is centered around developing open-source tooling (Dao et al., 2022; Kwon et al., 2023) to enable further scaling and understanding emergent behavior of such models (Schaeffer et al., 2023), including probing current limitations (Dziri et al., 2024).

Indeed, the rapid escalation of generative model development has also induced a democratizing effect, given the easy access to large pre-trained in the current AI climate (Stability AI, 2023; Midjourney, 2023; Ramesh et al., 2021). Furthermore, with the rise of open-source models, it is now easier than ever to host and deploy fine-tuned models. However, the current pace of progress also makes it infeasible to easily scale further models without confronting practical challenges. For instance, for continuous domains such as natural images current pre-trained diffusion models already exhaust all public data, with a growing proportion of the web already populated with synthetic data (Schuhmann et al., 2022). Compounding these challenges is the tremendous cost of pre-training these large diffusion models, which at present makes it computationally unattractive for individuals to build large pre-trained models on different datasets without re-training a larger combined model.

A compelling alternative to training ever larger models is to consider the efficacy of maximizing the utility of existing pre-trained models. In particular, it is interesting to consider the compositional benefits of combining pre-trained models at the generation stage in place of training a single monolithic model (Du & Kaelbling, 2024). For diffusion models, which are the current de facto modeling paradigm over continuous domains, compositional generation can be framed as modifying the inference mechanism through either guidance (Dhariwal & Nichol, 2021; Ho & Salimans, 2022) or applying complex MCMC correction schemes (Du et al., 2023). Despite advancements, methods that utilize guidance lack a firm theoretical underpinning (Bradley & Nakkiran, 2024) and MCMC techniques are prone to scaling issues, and more importantly, remain unproven at combining existing large pre-trained diffusion models. This motivates the following timely research question: ***Can we combine pre-trained diffusion models solely at inference in a theoretically sound and efficient manner?***

Present work. In this paper, we cast the problem of combining and composing multiple pre-trained diffusion models under a novel joint inference framework we term superposition. Intuitively we develop our framework by starting from the well-known principle of superposition in physical systems which summarizes the net response to multiple inputs in a linear system as the sum of individual inputs. Applying the superposition principle we develop SUPERDIFF, a novel approach to combine pre-trained diffusion models by superimposing learned vector fields at inference. Moreover, we demonstrate that the same superposition principle underlies both flow-based methods (Liu et al., 2022b; Lipman et al., 2022; Albergo et al., 2023) and diffusion models (Ho et al., 2020; Song et al., 2020) (see App. B), and thus provides a unifying perspective over combining modern generative models.

SUPERDIFF relies on the key insight that following a superposition principle necessitates the efficient evaluation of the densities of different models during the generation, which we present in Sec. 3.1. Knowing the current density of the generated sample under different models (or the same model with different conditioning) we are able to guide the generation to the desired result by controlling the relative weights of model outputs. Namely, in Sec. 3.2, we propose two different algorithms that implement: a mixture of densities (sampling from either from one model OR another), generating samples of the equal densities (samples that are likely under one model AND another, e.g. see Fig. 1).

We test the applicability of our approach SUPERDIFF using the two proposed superimposition strategies for image and protein generation tasks. For images, we first demonstrate the ability to combine the outputs of two models trained on disjoint datasets such that they yield better performance than the model trained on both of the datasets (see Sec. 4.1). In addition, we demonstrate the ability to interpolate between densities which correspond to concept interpolation in the image space (see Sec. 4.2). For proteins, we demonstrate that combining two different generative models leads to improvements in designability and novelty generation (see Sec. 4.3). Across all our experimental settings, we find that combining pre-trained diffusion models using SUPERDIFF leads to higher fidelity generated samples that better match task specification in text-conditioned image generation and also produce more diverse generated protein structures than comparable composition strategies.

2 PRELIMARIES

Generative models learn to approximate a target data distribution $p_{\text{data}} \in \mathbb{P}(\mathbb{R}^d)$ defined over $\mathbb{R}^d$ using a parametric model q_θ with learnable parameters θ. In the conventional problem definition, the data distribution is realized as an empirical distribution that is provided as a training set of samples

$\mathcal{D} = \{\mu^i\}_{i=1}^m$. Whilst there are multiple generative model families to choose from, we restrict our attention to diffusion models (Song et al., 2020; Ho et al., 2020) which are arguably the most popular modeling family driving current application domains. We next review the basics of the continuous time formulation of diffusion models before casting them within our superposition framework.

2.1 Continuous-time diffusion models

A diffusion model can be cast as the solution to the Stochastic Differential Equation (Øksendal, 2003),

$$dx_t = f_t(x)dt + g_t dW_t, \quad x_0 \sim q_0(x_0). \tag{1}$$

In the Itô SDE literature, the function $f_t : \mathbb{R}^d \to \mathbb{R}^d$ is known as the drift coefficient while $g_t : \mathbb{R} \to \mathbb{R}$ is a real-valued function called the diffusion coefficient and W_t is the standard Wiener process. The subscript index $t \in [0, 1]$ indicates the time-valued nature of the stochastic process. Specifically, we fix the starting time $t = 0$ to correspond to the data distribution $p_{\text{data}} := q_0(x_0)$ and set $t = 1$ as the terminal time $t = 1$ to an easy to sample prior such as a standard Normal distribution $p_{\text{noise}} := q_1(x_1) = \mathcal{N}(x_1|0, I)$. As such the diffusion SDE, also called the forward process, can be seen as progressively corrupting the data distribution and ultimately hitting a terminal distribution devoid of any structure.

To generate samples from the marginal density $q_t(x_t)$ induced by the diffusion SDE in equation 1 we leverage the reverse-time SDE with the same marginal density as demonstrated below.

Proposition 1. [Reverse-time SDEs/ODE] *Marginal densities $q_t(x)$ induced by Eq. (1) correspond to the densities induced by the following SDE that goes back in time ($\tau = 1 - t$) with the corresponding initial condition*

$$dx_\tau = \left(-f_t(x_\tau) + \left(\frac{g_t^2}{2} + \xi_\tau\right)\nabla \log q_t(x_\tau)\right)d\tau + \sqrt{2\xi_\tau}d\overline{W}_\tau\,, \quad x_{\tau=0} \sim q_1(x_0)\,, \tag{2}$$

where $\overline{W}_\tau$ is the standard Wiener process in time τ, and ξ_τ is any positive schedule.

See proof in App. A.1. The reverse SDE flows backward in time $\tau = 1 - t$ and is linked to the diffusion SDE through the score $\nabla_x \log q_\tau(x)$, and $d\overline{W}_\tau$ is another Weiner process. As a result, a parametric model $\nabla \log q_\tau(x; \theta)$ may directly learn to approximate this score function for every point in time and then draw samples by simulating the reverse SDE in equation 2 by plugging back in the learned score. Notably, for $\xi_t \equiv 0$, the SDE becomes an ODE which defines a smooth change of measure corresponding to p_{noise} into the measure corresponding to p_{data}.

In practice, for generative modelling, the forward SDE from Eq. (1) is chosen to be so simple that it can be integrated in time analytically without simulating the SDE itself. This is equivalent to choosing the noising schedule first, and then deriving the SDE that corresponds to this schedule. Namely, for every training sample μ^i, we can define the density of the corrupted μ^i as a normal density with the mean scaled according to α_t and the variance σ_t^2, then the density of the entire corrupted dataset is simply a mixture over all training samples μ^i, i.e.

$$q_t^i(x) = \mathcal{N}(x \,|\, \alpha_t \mu^i, \sigma_t^2 I)\,, \quad q_t(x) = \frac{1}{N}\sum_{i=1}^{N} q_t^i(x)\,. \tag{3}$$

Clearly, choosing α_t, σ_t such that $\alpha_0 = 1, \sigma_0 = 0$ and $\alpha_1 = 0, \sigma_1 = 1$, we guarantee $p_{\text{data}} := q_0(x_0)$ and $p_{\text{noise}} := q_1(x_1) = \mathcal{N}(x_1|0, I)$. This perturbation of the data distribution using a Gaussian kernel offers specific forms for the drift f_t, and diffusion coefficient g_t as described next.

Proposition 2. [Ornstein–Uhlenbeck SDE] *The time-dependent densities in Eq. (3) correspond to the marginal densities of the following SDE, with the corresponding initial condition*

$$dx_t = \underbrace{\frac{\partial \log \alpha_t}{\partial t} x_t}_{f_t(x_t)} dt + \underbrace{\sqrt{2\sigma_t^2 \frac{\partial}{\partial t} \log \frac{\sigma_t}{\alpha_t}}}_{g_t} dW_t\,, \quad x_0 \sim q_0(x_0)\,. \tag{4}$$

See proof in App. A.2. We highlight the simplicity of the drift term, a linear scaling, that allows us to simulate efficiently the reverse SDE and is crucial for the proposed density estimators in Sec. 3.1. Altogether, the derivations of this section allow us to go from the noise schedules of samples

in Eq. (3) used during the training of a given diffusion model to the corresponding forward SDE in Prop. 2, and finally to the reverse SDEs or ODE used in Prop. 1.

2.2 Superposition of ODEs and SDEs

In this section, we introduce the superposition of multiple time-dependent densities that correspond to different stochastic processes. A suggestive view of these densities is as processes corresponding to different training data (e.g. different datasets), different conditions (e.g. different text prompts), or simply differently trained diffusion models. Namely, we consider N forward noising process $\{q_t^i(x)\}_{i=1}^N$ that possibly start from different initial distributions $\{q_{t=0}^i(x)\}_{i=1}^N$ (e.g. different datasets). Assume that we know the individual vector fields $v_t^i(x)$ that define the change of corresponding densities $q_t^i(x)$ via the state-space ODEs and continuity equations,

$$\frac{dx_t}{dt} = v_t^i(x_t) \quad \Longrightarrow \quad \frac{\partial}{\partial t} q_t^i(x) = -\left\langle \nabla_x, q_t^i(x) v_t^i(x) \right\rangle, \quad \forall\, i \in [N]. \tag{5}$$

The *superposition* of the noising processes $\{q_t^i(x)\}_{i=1}^N$ is the mixture of corresponding densities:

$$q_t^{\text{mix}}(x) := \sum_{j=1}^N \omega^j q_t^j(x), \quad \sum_{i=1}^N \omega^i = 1\,, \quad \omega^i \geq 0\,, \tag{6}$$

where ω^j is a mixing coefficient. Note that superimposed $q_t^{\text{mix}}(x)$ also satisfies the continuity equation for the superposition of the vector fields $v_t^i(x)$ as demonstrated in the following proposition.

Proposition 3. [Superposition of ODEs (Liu, 2022)] *The mixture density in Eq. (6) follows the continuity equation with the superposed vector fields from Eq. (5), i.e.*

$$\frac{\partial}{\partial t} q_t^{\text{mix}}(x) = -\left\langle \nabla_x, q_t^{\text{mix}}(x) v_t(x) \right\rangle, \quad v_t(x) = \frac{1}{\sum_{j=1}^N \omega^j q_t^j(x)} \sum_{i=1}^N \omega^i q_t^i(x) v_t^i(x)\,. \tag{7}$$

We reproduce the proof for Prop. 3 in the context of our superposition in App. A.3. The superposition principle is the core principle that allows for efficient simulation-free learning of the flow-based models (Liu et al., 2022b; Lipman et al., 2022; Albergo et al., 2023) and diffusion models (Song et al., 2020). We discuss how these frameworks are derived from the superposition principle in App. B.

The superposition principle straightforwardly extends to the marginal densities of SDEs. That is, consider marginals densities $q_\tau^i(x)$ generated by the following SDEs

$$dx_\tau = u_\tau^i(x_\tau)d\tau + g_\tau d\overline{W}_\tau\,, \quad x_{\tau=0} = q_{\tau=0}^i(x_0)\,, \tag{8}$$

where one has to note the same diffusion coefficient for all the SDEs. Then the mixture of densities from Eq. (6) can be simulated by the SDE from the following proposition.

Proposition 4. [Superposition of SDEs] *The mixture $q_t^{\text{mix}}(x) := \sum_{i=1}^N \omega^i q_t^i(x)$ of density marginals $\{q_t^i(x)\}_{i=1}^N$ induced by SDEs from Eq. (8) corresponds to the following SDE*

$$dx_\tau = u_\tau(x_\tau)d\tau + g_\tau d\overline{W}_\tau\,, \quad u_t(x) = \frac{1}{\sum_{j=1}^N \omega^j q_t^j(x)} \sum_{i=1}^N \omega^i q_t^i(x) u_t^i(x)\,. \tag{9}$$

See App. A.4 for the proof. Both Prop. 3 and Prop. 4 can be easily extended to the families of densities parameterized with a continuous variable, but this is beyond the scope of the current paper.

3 Superposition of different models

We now introduce our method for combining pre-trained diffusion models using the principle of superposition. The result of this is a novel inference time algorithm SuperDiff which can be easily applied without further fine-tuning or post-processing of any of the pre-trained diffusion weights. Our proposed approach SuperDiff can be instantiated in two distinct ways that allow for the composition diffusion models that can be informally interpreted as logical composition operators in the logical AND and the logical OR. More precisely, given two pre-trained diffusion models that are trained on datasets A and B inference using SuperDiff can be done by either sampling from the mixture of the two learned densities, i.e. logical AND Fig. 2c, or sampling from the equal density locus (logical OR Fig. 2d). In such a manner, superposition using AND leads to generated samples that are equally likely

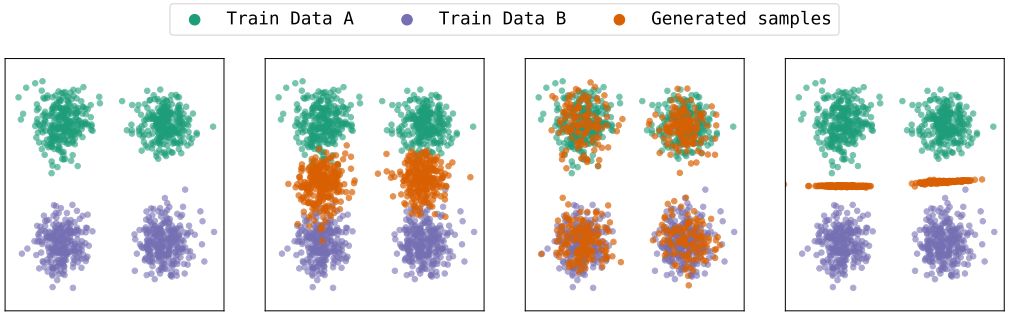

(a) Training datasets (b) Averaging the vector fields (c) Sampling the mixture of densities **(ours)** (d) Sampling equal densities **(ours)**

Figure 2: An intuitive illustration of using model superposition for improving inference performance. We show an example of two disjoint datasets and train a model for each set. Each individual model learns to generate samples only from their respective datasets. Using model superposition enables sampling from both densities.

under both pre-trained diffusion models while superposition using OR creates samples that are preferentially generated by either pre-trained model—and thus mimics the empirical distributions A or B.

Method overview. SUPERDIFF is applicable in settings where the modeler has access to M pre-trained diffusion models, along with its learned score function $\nabla_x \log q_t^i(x)$. Each of the pre-trained models follows a marginal density $q_t^i(x)$ and as a result must admit a corresponding vector field $v_t^i(x)$ that satisfies the continuity equation in Equation 5. The key idea of our approach is an adaptive re-weighting scheme of the pre-trained model's vector fields that relies on the likelihood of a sample under different models. A naive approach to estimating each marginal density during generation immediately presents several technical challenges as it requires the estimation of the divergence of superimposed vector fields. In particular, these challenges can be stated as follows:

(C1) The marginal superpositioned vector field differs from the vector fields of either of the models.
(C2) The divergence operation requires backpropagation through the network and is computationally expensive even with Hutchinson's trace estimator (Hutchinson, 1989).

Our proposed approach SUPERDIFF overcomes these computational challenges by introducing a novel density estimator in Sec. 3.1. Crucially, this new estimator does not require divergence estimation and enjoys having the same variance as the computationally expensive Hutchinson's trace estimator, making it a favorable choice when generating using large pre-trained diffusion models. In section Sec. 3.2 we exploit this new density estimator to formally present our algorithm SUPERDIFF and derive connections to the composition operators that intuitively resemble logical AND and OR.

3.1 EVALUATING THE DENSITIES ON THE FLY

In this section, we introduce a novel method for evaluating the marginal density of a diffusion model during the inference process. The conventional way to evaluate the density uses the continuity equation and solves the same ODE that is used for generating samples. This, however, is not easily possible in the case of our superposition of vector fields framework as outlined in Prop. 3. To solve this, we present the following proposition that disentangles the vector field generating the sample ($u_t(x)$ in the proposition) and the vector fields corresponding to different generative models $v_t^i(x)$.

Proposition 5. [Smooth density estimator] *For the integral curve $x(t)$ solving $dx/dt = u_t(x_t)$, and the density $q_t^i(x(t))$ satisfying the continuity equation $\frac{\partial}{\partial t} q_t^i(x) = -\langle \nabla_x, q_t^i(x) v_t^i(x) \rangle$, the log-density along the curve changes according to the following ODE*

$$\frac{d}{dt} \log q_t^i(x(t)) = -\langle \nabla_x, v_t^i(x) \rangle - \langle \nabla_x \log q_t^i(x), v_t^i(x) - u_t(x) \rangle . \tag{10}$$

See proof in App. C. We use this proposition for our experiments conducted in Sec. 4.1. However, as outlined previously, evaluating the marginal density via the continuity equation is restricted to small-scale models due to the computational challenges associated with efficiently estimating the divergence of the associated vector field. As a result, a common line of attack assumes constructing

Algorithm 1: SUPERDIFF pseudocode (for **OR** and **AND** operations)

Input : M pre-trained score models $\nabla_x \log q_t^i(x)$, the parameters of the schedule α_t, σ_t, stepsize $d\tau > 0$, temperature parameter T, bias parameter ℓ, and initial noise $z \sim \mathcal{N}(\mathbf{0}, \mathbf{I})$.

for $\tau = 0, \ldots, 1$ **do**

$t = 1 - \tau, \quad \varepsilon \sim \mathcal{N}(\mathbf{0}, \mathbf{I})$

$$\kappa_\tau^i \leftarrow \begin{cases} \texttt{softmax}(T \log q_t^i(x_\tau) + \ell) & \texttt{// for OR according to Prop. 3} \\ \texttt{solve Linear Equations} & \texttt{// for AND according to Prop. 6} \end{cases}$$

$u_t(x) \leftarrow \sum_{i=1}^M \kappa_\tau^i \nabla \log q_t^i(x_\tau)$

$dx_\tau \leftarrow \big(-f_{1-\tau}(x_\tau) + g_{1-\tau}^2 u_t(x)\big)d\tau + g_{1-\tau} d\overline{W}_\tau$ // using Prop. 1

$x_{\tau+d\tau} \leftarrow x_\tau + dx_\tau$

$$d \log q_{1-\tau}(x_\tau) = \big\langle dx_\tau, \nabla \log q_{1-\tau}(x_\tau)\big\rangle + \Bigg(\big\langle \nabla, f_{1-\tau}(x_\tau)\big\rangle + \\ + \Bigg\langle f_{1-\tau}(x_\tau) - \tfrac{g_{1-\tau}^2}{2} \nabla \log q_{1-\tau}(x_\tau), \nabla \log q_{1-\tau}(x_\tau)\Bigg\rangle\Bigg) d\tau \quad \texttt{// using Thm. 1}$$

return x

a stochastic unbiased estimator that trades for increased speed by introducing a bit of variance into the divergence estimate. This approach is known as Hutchinson's estimator and requires computing a Jacobian-vector product at every step of the inference.

Instead, we propose a new way to estimate density that allows for efficient computation while integrating the backward SDE from Prop. 1 with a specific choice of the diffusion coefficient.

Theorem 1. [Ôti density estimator] *Consider time-dependent density $q_t(x)$ induced by the marginals of the following "forward" process*

$$dx_t = f_t(x_t)dt + g_t dW_t\,, \quad x_{t=0} \sim q_0(x)\,, \quad t \in [0, 1]\,, \tag{11}$$

where dW_t is the Wiener process. Then, for the following "backward" SDE (with $\tau = 1 - t$)

$$dx_\tau = u_\tau(x_\tau)d\tau + g_{1-\tau} d\overline{W}_\tau\,, \quad \tau \in [0, 1]\,, \tag{12}$$

the change of the log-density $\log q_\tau(x_\tau)$ follows the following SDE

$$d \log q_{1-\tau}(x_\tau) = \big\langle dx_\tau, \nabla \log q_{1-\tau}(x_\tau)\big\rangle + \Bigg(\big\langle \nabla, f_{1-\tau}(x_\tau)\big\rangle + \\ + \Bigg\langle f_{1-\tau}(x_\tau) - \frac{g_{1-\tau}^2}{2} \nabla \log q_{1-\tau}(x_\tau), \nabla \log q_{1-\tau}(x_\tau)\Bigg\rangle\Bigg) d\tau\,. \tag{13}$$

We provide the proof in App. C. Notably, the SDE Eq. (13) that keeps track of the change of log-density does not include only the divergence of the forward SDE drift $\langle \nabla, f_{1-\tau}(x_\tau)\rangle$. However, in practice, when using the Ornstein-Uhlenbeck SDE, this divergence is simply a constant because the drift term is a linear scaling. In App. D, we derive the same estimator but in discrete time using the detailed balance condition.

3.2 SUPERDIFF: SUPERPOSING PRE-TRAINED DIFFUSION MODELS

Mixture of densities (logical OR). For a mixture of the densities, superposition of the models follows directly from the propositions in Sec. 2.2. That is, for every $q_t^i(x)$, we assume that it can be generated from SDEs or an ODE from Prop. 1 and we assume the knowledge of scores $\nabla \log q_t^i(x)$.

Then, for the ODE simulation, according to Prop. 3, we can sample from the mixture of densities $q_t^{\text{mix}}(x) := 1/M \sum_{i=1}^M q_t^i(x)$ using the following vector field

$$v_\tau(x) = -f_{1-\tau}(x) + \frac{g_{1-\tau}^2}{2} \sum_{i=1}^M \frac{q_t^i(x)}{\sum_j q_t^j(x)} \nabla \log q_{1-\tau}^i(x)\,, \tag{14}$$

starting from samples $x_{\tau=0} \sim q_1(x_0)$. The densities are estimated along the trajectory using Prop. 5.

We highlight this analogously applies for simulation using the SDE $dx_\tau = u_\tau(x_\tau)d\tau + g_{1-\tau}d\overline{W}_\tau$. Namely, according to Prop. 4, we use the following vector field:

$$u_\tau(x) = -f_{1-\tau}(x) + g_{1-\tau}^2 \sum_{i=1}^{M} \frac{q_t^i(x)}{\sum_j q_t^j(x)} \nabla \log q_{1-\tau}^i(x)\,, \tag{15}$$

starting from the samples $x_{\tau=0} \sim q_1(x_0)$. The densities are estimated along the trajectory using Thm. 1. We provide the pseudocode in Algorithm 1.

Sampling equal densities (logical AND). To produce the sample that have equal densities under different models we rely on our formula for the density update (see Thm. 1) to find the optimal weights for the vector fields. Indeed, for M diffusion models, we have a system of M equations: the equal change of density for every model and the normalization constraint for model weights, which is a linear system w.r.t. vector field weights as we show in the following proposition.

Proposition 6. [Density control] *For the SDE*

$$dx_\tau = \sum_{j=1}^{M} \kappa_j u_\tau^j(x_\tau)d\tau + g_{1-\tau}d\overline{W}_\tau\,, \tag{16}$$

where κ are the weights of different models and $\sum_j \kappa_j = 1$, one can find κ that satisfies

$$d\log q_{1-\tau}^i(x_\tau) = d\log q_{1-\tau}^j(x_\tau)\,, \quad \forall\ i,j \in [M]\,, \tag{17}$$

by solving a system of M linear equations w.r.t. κ.

We provide the proof and the formulas for the system of linear equations in App. C.1. This proposition allows us to find κ that controls the densities to stay the same for all the models as described in Algorithm 1. This approach can also be straightforwardly extended to the case of diffusion models for satisfying different prescribed density ratios, i.e.

$$d\log q_{1-\tau}^1(x_\tau) = d\log q_{1-\tau}^i(x_\tau) + \ell^i\,. \tag{18}$$

4 Experiments

4.1 Joining models with disjoint training data

We validate the proposed Algorithm 1 for the generation of the mixture of the distributions (OR setting). We split CIFAR-10 into two disjoint training sets of equal size (first 5 labels and last 5 labels), train two diffusion models on each part, and generate the samples jointly using both models. Namely, the stochastic inference is the OR implementation of Algorithm 1, whereas the deterministic setting is the integration of the ODEs (see Prop. 1) and the estimation of the log-density according to Prop. 5. For the choice of hyperparameters, architecture, and data preprocessing, we follow (Song et al., 2020).

In Table 1, we demonstrate that the performance of SuperDiff drastically outperforms the performance of the individual models and performs even better than the model trained on the union of both parts of the dataset. For comparison, we evaluate conventional image quality metrics (Frechet inception distance (FID), Inception score (IS), and feature likelihood divergence (FLD) (Jiralerspong et al., 2023), which takes into account the generalization abilities of the model.[1]

4.2 Concept interpolation and selection with SuperDiff and Stable Diffusion

Next, we evaluate the ability of SuperDiff to interpolate (logical AND) or select (logical OR) different concepts using prompt-conditioned Stable Diffusion (SD). In this setup, we generate images from SD by conditioning it on a prompt using classifier-free guidance. We define two models using two separate prompts that represent concepts — e.g. `"a sunflower"` and `"a lemon"`. We can thus consider each prompt-conditioned model as a separate diffusion model and apply Algorithm 1 to generate images sampled with proportionally equal likelihood with respect to both prompt-conditioned models (logical AND), or to generate from the mixture of distributions (logical OR). We generate 20 images for 20 different concept pairs (tasks) for our model and baselines (c.f. App. H)).

[1] In Table 1, we report results for both the SDE and the ODE inference. However, we note that for the ODE setting, evaluating densities takes about 4x longer than our density estimator in the SDE setting and requires 1.5x more memory, and so we carry out remaining experiments only using SDEs.

Table 1: Image generation performance for CIFAR-10 with *unconditional* models trained on two disjoint partitions of the training data (labeled A and B). We compare SUPERDIFF (**OR**) with the respective models (model$_A$ and model$_B$) with the model that is trained on the full dataset (model$_{A \cup B}$) and random choice between two models (model$_{A \text{ OR } B}$).

	ODE inference			SDE inference		
	FID (↓)	IS (↑)	FLD (↓)	FID (↓)	IS (↑)	FLD (↓)
model$_A$	14.00	8.73	15.50 ± 0.17	15.33	7.98	15.47 ± 0.18
model$_B$	13.09	7.89	18.90 ± 0.18	13.50	7.98	18.54 ± 0.23
model$_{A \cup B}$	6.00	8.95	8.06 ± 0.12	**3.50**	9.14	7.51 ± 0.11
model$_{A \text{ OR } B}$	4.28	9.14	5.96 ± 0.11	3.99	9.36	5.29 ± 0.14
SUPERDIFF (**OR**)	4.41	9.12	6.10 ± 0.11	4.00	9.36	5.33 ± 0.05
SUPERDIFF $_{T=100}$ (**OR**)	**4.11**	**9.21**	$\mathbf{5.89 \pm 0.11}$	4.00	**9.48**	$\mathbf{5.20 \pm 0.11}$

Table 2: Quantativate evaluation of SD-generated images. For logical **AND**, we compare SUPERDIFF (**AND**), joint prompting, and averaging of outputs for two concept prompts. We report the minimum CLIP, ImageReward, and TIFA scores from the two concept prompts, which gives a measure of how well each method represents both concepts. For logical **OR**, we compare SUPERDIFF (**OR**), joint prompting, and an upper bound of randomly selecting a single concept prompt (Prompt$_{A \text{ OR } B}$). We report the maximum scores from each prompt pair, as well as the absolute difference between the maximum and minimum scores ($|\Delta|$). These metrics reflect how well a method can select one concept to generate.

	Min. CLIP (↑)	Min. ImageReward (↑)	Min. TIFA (↑)
Joint prompting	23.87	−1.62	27.58
Average of scores (Liu et al., 2022a)	24.23	−1.57	32.48
SUPERDIFF (**AND**)	**24.79**	**−1.39**	**39.92**
	$\lvert\Delta\rvert$/Max. CLIP (↑)	$\lvert\Delta\rvert$/Max. ImageReward (↑)	$\lvert\Delta\rvert$/Max. TIFA (↑)
Prompt$_{A \text{ OR } B}$ (uncorrelated random choice)	9.13/29.72	2.87/0.70	88.21/97.58
Joint prompting	7.20/29.80	2.47/0.59	79.46/**97.92**
SUPERDIFF (**OR**)	**8.58**/**29.87**	**2.76**/**0.64**	**84.10**/95.83

Baselines for concept interpolation (AND). We consider two approaches for composing images as baselines. The first is simple averaging of SD outputs based on the approach in (Liu et al., 2022a); we set $\kappa = 0.5$. The second guides SD generation with a single joint prompt that encourages SD to interpolate concepts. The prompts are constructed by joining two input concepts with the linking term `"that looks like"`. For example, given the concepts `"a sunflower"` and `"a lemon"`, the prompt is `"a sunflower that looks like a lemon"`. For fairness, we also flip the order of the prompt and keep the image with the higher score for all metrics listed below (Luo et al., 2024).

Baselines for concept selection (OR). For the **OR** setting, our baseline is prompting SD that prompts the model to select between two concepts: `"a sunflower or a lemon"`. As with **AND**, we also flip the prompt and keep the better image for each metric. As an upper bound, we generate images from SD by prompting it with a random choice between the two concepts (Prompt$_{A \text{ OR } B}$).

SUPERDIFF qualitatively generates images with better concept interpolations and selections. We plot sample generated images for SUPERDIFF (**AND**) in Fig. 1. For the complete set of generated images, see App. H (Figs. A1–A20). We observe that SUPERDIFF (**AND**) can interpolate concepts while also maintaining high perceptual quality. In contrast, the averaging baseline either fails to interpolate concepts form both prompts fully, are yields images with lower perceptual quality. We observe that SD using a single prompt struggles to interpolate both concepts.

For concept selection (**OR**), we find that SUPERDIFF (**OR**) can faithfully generate images with a single concept. The joint prompting baseline can sometimes generate images that combine fragments of both concepts, but other times it also generates images of a single concept, typically the first concept in the joint prompt (this also underscores why this method struggles with concept interpolation). We show examples of these cases in Fig. A21.

SUPERDIFF outperforms baselines on three image evaluation metrics. To quantitatively evaluate the generated images, we consider three metrics: CLIP Score (Radford et al., 2021), ImageReward (Xu et al., 2024), and TIFA (Hu et al., 2023). CLIP Score measures the cosine similarity between an image embedding and text prompt embedding. ImageReward evaluates generated images by assigning a score that reflects how closely they align with human preferences, including aesthetic quality and prompt adherence. TIFA generates several question-answer pairs using a Large Language Model for a given prompt and assigns a score by answering the questions based on the image with a visual question-answering model. We report these metrics for SUPERDIFF and all baselines in Table 2.

Table 3: Evaluation of SUPERDIFF and baseline models, Proteus & FrameDiff, for unconditional protein generation. We show results for three categories of metrics: designability, novelty, and diversity. We also include a baseline of simple averaging of scores ($\kappa = 0.5$). We use the parameter ℓ (see Eq. (18)) to control and bias model superposition towards Proteus, i.e. ($\ell > 0$) or FrameDiff ($\ell < 0$). We use temperature values $T = 1$ for all variants of SUPERDIFF. For each type of model composition (averaging or SUPERDIFF), we mark each metric with a (†) if it is better than both Proteus and FrameDiff on their own, and with a ($\star$) if it better than either one of them.

	Designability		**Novelty**			**Diversity**		
	< 2Å scRMSD (↑)	scRMSD (↓)	< 0.5 scTM (↑)	< 0.3 scTM (↑)	Max. scTM (↓)	Frac. β (↑)	Pairwise scTM (↓)	Max. cluster (↑)
FrameDiff	0.392 ± 0.03	4.315 ± 0.25	0.152 ± 0.02	0.016 ± 0.01	0.570 ± 0.02	$\mathbf{0.175 \pm 0.01}$	0.337 ± 0.02	$\mathbf{0.326 \pm 0.05}$
Proteus	0.928 ± 0.02	1.014 ± 0.07	0.360 ± 0.03	0.020 ± 0.01	0.536 ± 0.01	0.119 ± 0.01	0.312 ± 0.01	0.217 ± 0.02
Average of scores (Liu et al., 2022a)	$0.740 \pm 0.03^\star$	$1.960 \pm 0.14^\star$	$0.360 \pm 0.03^\star$	$0.024 \pm 0.01^\dagger$	$\mathbf{0.511 \pm 0.01}^\dagger$	$0.139 \pm 0.01^\star$	$0.310 \pm 0.01^\dagger$	$0.253 \pm 0.01^\star$
SUPERDIFF$_{\ell=0}$(OR)	$0.752 \pm 0.03^\star$	$1.940 \pm 0.14^\star$	$0.276 \pm 0.03^\star$	0.008 ± 0.01	$0.547 \pm 0.01^\star$	$0.147 \pm 0.01^\star$	$\mathbf{0.309 \pm 0.02}^\dagger$	$0.268 \pm 0.02^\star$
SUPERDIFF$_{\ell=1}$(OR)	$\mathbf{0.976 \pm 0.01}^\dagger$	$\mathbf{0.929 \pm 0.05}^\dagger$	$\mathbf{0.396 \pm 0.03}^\dagger$	$0.024 \pm 0.01^\dagger$	$0.528 \pm 0.01^\dagger$	$0.127 \pm 0.01^\star$	$\mathbf{0.307 \pm 0.02}^\dagger$	$0.246 \pm 0.03^\star$
SUPERDIFF$_{\ell=0}$(AND)	$0.740 \pm 0.03^\star$	$2.119 \pm 0.16^\star$	$0.320 \pm 0.03^\star$	$\mathbf{0.044 \pm 0.01}^\dagger$	$0.513 \pm 0.01^\dagger$	$0.142 \pm 0.01^\star$	$0.310 \pm 0.02^\dagger$	$0.265 \pm 0.01^\dagger$

For the logical **AND** setting, we evaluate the image against each concept prompt separately (i.e., "a sunflower" as one prompt and "a lemon" as the other) and take the minimum score for each metric. This is so that we can measure how well *both* concepts are represented. We find that SUPERDIFF (**AND**) obtains the highest scores across all metrics, indicating that our method can better represent both concepts in the images, while the baseline methods typically only represent one concept or (especially in the case of averaging outputs), generate compositions with lower fidelity. For the logical **OR** setting, we again evaluate the image against each concept prompt separately and take both the maximum score and the absolute difference between both scores for each metric. This is so that we can measure how well *one* concept is represented. The upper bound for this setting is randomly prompting SD with either of the prompts; we find that we are almost able to match this setting across all scores, indicating that our method is able to faithfully select a single concept. SD with joint prompting does not perform as well, as nothing prevents it from combining components from both concepts.

4.3 PROTEIN GENERATION

Finally, we apply our method in the setting of unconditional *de novo* protein generation. Protein generation has critical implications in drug discovery (Abramson et al., 2024). A good understanding of the protein landscape is important to rationally find novel proteins.

We evaluate proteins generated by the superposition of two existing protein diffusion models, Proteus (Wang et al., 2024) and FrameDiff (Yim et al., 2023b), in terms of their *designability*, *novelty*, and *diversity*, following metrics from Bose et al. (2024). We report the results of our best model in Table 3, as well as results for each model individually and simply averaging them. All results are averages over 50 generated proteins at lengths $\{100, 150, 200, 250, 300\}$ for 500 timesteps.

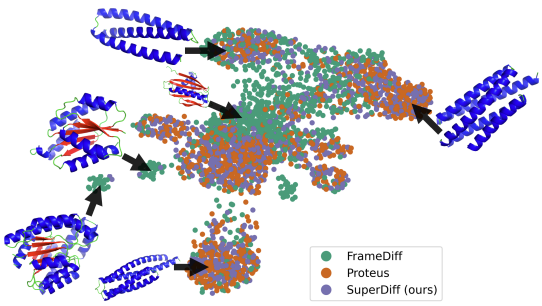

Figure 3: UMAP visualization of protein structures showing cluster archetypes where structure diversity is maintained with SUPERDIFF $\ell=1$ (**OR**).

Metrics for evaluations. We consider *designability*, *novelty*, and *diversity* metrics for evaluation of unconditional generation of protein structures. Protein *designability* refers to the in-silico agreement between generated structures and refolded structures as computed using a purpose-built folding model e.g. ESMFold (Lin et al., 2022), which is positively correlated with the synthesizability of the protein in a wet-lab setting. Generally, if the root-mean-square distance between the generated and refolded proteins (scRMSD) is less than 2Å, it is considered to be designable. We provide details of all metrics in this section in App. G.2.

We compute several *novelty* metrics based on the similarity of generated proteins to those from the set of known proteins (the training set), which are called scTM scores; the lower the score, the less similar the generated protein is to the training data. Lastly, we use *diversity* to assess the degree of heterogeneity present in the set of generated proteins. This is done by clustering the generated proteins in terms of sequence overlap, and measuring the fraction of proteins with challenging-to-generate secondary structures such as β sheets (Bose et al., 2024).

SUPERDIFF improves structure generation. By combining two protein diffusion models, SUPERDIFF is able to outperform both of them. This is somewhat surprising as FrameDiff is substantially less designable than Proteus (0.392 vs. 0.928 scRMSD) (see Table 3). Nevertheless, by using SUPERDIFF (**OR**), we can increase designability, novelty, and maintain diversity. We also find that SUPERDIFF (**OR**) substantially outperforms simple averaging, which simply mixes the performance of the two models, and does not improve over either one.

We also find that SUPERDIFF (**AND**) can match averaging in terms of designability while improving diversity. Perhaps more impressively, SUPERDIFF (**AND**) can generate the most proteins that are furthest away from the set of known proteins (scTM score < 0.3) by almost two times more than the next best method. This motivates the utility of applying our method in novel discovery settings.

We further investigate the composition made by SUPERDIFF (**OR**) in Fig. 3. Here, we see a few modes (particularly on the plot's left-hand side) that Proteus does not generate. We find that SUPERDIFF (**OR**) can maintain knowledge of these clusters (although to a lesser extent) while maintaining designability.

5 RELATED WORK

Compositional diffusion models. Combining multiple density models into one model with better properties is a classical subject in machine learning (Hinton, 2002). For diffusion models, the most straightforward combination is via averaging their respective learned score functions (Liu et al., 2022a; Kong et al., 2024), which can also be viewed as a form of guidance (Ho et al., 2020; Dhariwal & Nichol, 2021; Bansal et al., 2023). Another way to combine diffusion models comes from their connections to energy-based models (Du et al., 2023; 2020; Nie et al., 2021; Ajay et al., 2024). This, however, comes under a strong assumption that the marginal densities of the noising process are given, which is not the case in most of the modern applications (e.g. Rombach et al. (2022)); our method resolves this. Density estimation, also, is the main bottleneck for the continual learning of diffusion models, e.g. Golatkar et al. (2023) proposes to learn a separate model for the densities in order to simulate the vector fields from Prop. 3. Finally, some works (Zhong et al., 2024; Biggs et al., 2024) propose to combine models by averaging their weights. This does not allow for merging of the models with different architectures (as we do in Sec. 4.3) and does not allow for merging the same model with different conditions (as we do in Sec. 4.2).

Protein generation. Structure-based de novo protein design using deep generative models has recently seen a surge in interest, with a particular emphasis on diffusion-based approaches (Watson et al., 2023; Yim et al., 2023b), and also flow matching methods (Bose et al., 2024; Yim et al., 2023a; 2024; Huguet et al., 2024). Moreover, building on the initial $\mathrm{SE}(3)$ equivariant diffusion paradigm multiple recent approaches have sought to increase the performance of the methods through architectural innovations (Wang et al., 2024), conditioning on auxiliary modalities such as sequence or sidechains (Ingraham et al., 2023; Lin et al., 2024). Finally, recent approaches tackle the problem of co-generation which seeks to define a joint inference procedure over both structure and sequences (Campbell et al., 2024; Ren et al., 2024; Lisanza et al., 2023), but remains distinct from the setting of this work which attempts to combine different pre-trained models using superposition.

6 CONCLUSION

Despite the ubiquity of diffusion models, many possible ways of performing generation remain unexplored, with classifier-free guidance being the only practical option (Ho & Salimans, 2022). In this paper, we address this shortcoming by proposing two novel methods for combining different models (or the same model with different condition variables) using SUPERDIFF for joint generation.

Limitations. While computationally efficient SUPERDIFF is still limited by the computational budget required to produce the outputs of each model. In particular, the combination at the level of model outputs cannot be simply done via cheap combinations of pre-trained model weights. This, however, invites us to develop a more principled—architecture and training-agnostic—method that does not require any assumptions prior assumptions which makes SUPERDIFF a general purpose method.

Future Work. Our method unlocks novel research directions by allowing for the principled generation of novel samples that were not previously possible to generate easily Sec. 4.2. Furthermore, we argue that the proposed way to estimate the density during the generation enables numerous new potential ways to control the generation process by providing the information about the likelihoods. We discuss the broader impacts of this work in App. E.

REPRODUCIBILITY STATEMENT

To facilitate reproducibility of our empirical results and findings, we intend to make our code publicly available in the final version. We describe all mathematical and algorithmic details necessary to reproduce our results throughout this paper. In Sec. 3 we outline the theoretical basis and mathematical framework for our method. Furthermore, we provide pseudocode for our method in Algorithm 1. For our theoretical contributions, we provide detailed proofs for all theorems and propositions in App. A, App. B and App. C. We provide experimental details for the CIFAR-10 image experiment results in Sec. 4.1. Details regarding experiments for concept interpolation via Stable Diffusion are discussed in Sec. 4.2 and App. H. Experimental details for unconditional protein generation are described in Sec. 4.3 and App. G.1.

REFERENCES

Josh Abramson, Jonas Adler, Jack Dunger, Richard Evans, Tim Green, Alexander Pritzel, Olaf Ronneberger, Lindsay Willmore, Andrew J Ballard, Joshua Bambrick, et al. Accurate structure prediction of biomolecular interactions with alphafold 3. *Nature*, pp. 1–3, 2024.

Josh Achiam, Steven Adler, Sandhini Agarwal, Lama Ahmad, Ilge Akkaya, Florencia Leoni Aleman, Diogo Almeida, Janko Altenschmidt, Sam Altman, Shyamal Anadkat, et al. Gpt-4 technical report. *arXiv preprint arXiv:2303.08774*, 2023.

Anurag Ajay, Seungwook Han, Yilun Du, Shuang Li, Abhi Gupta, Tommi Jaakkola, Josh Tenenbaum, Leslie Kaelbling, Akash Srivastava, and Pulkit Agrawal. Compositional foundation models for hierarchical planning. *Advances in Neural Information Processing Systems*, 36, 2024.

Michael S Albergo, Nicholas M Boffi, and Eric Vanden-Eijnden. Stochastic interpolants: A unifying framework for flows and diffusions. *arXiv preprint arXiv:2303.08797*, 2023.

Arpit Bansal, Hong-Min Chu, Avi Schwarzschild, Soumyadip Sengupta, Micah Goldblum, Jonas Geiping, and Tom Goldstein. Universal guidance for diffusion models. In *Proceedings of the IEEE/CVF Conference on Computer Vision and Pattern Recognition*, pp. 843–852, 2023.

Helen M Berman, John Westbrook, Zukang Feng, Gary Gilliland, Talapady N Bhat, Helge Weissig, Ilya N Shindyalov, and Philip E Bourne. The protein data bank. *Nucleic acids research*, 28(1): 235–242, 2000.

Benjamin Biggs, Arjun Seshadri, Yang Zou, Achin Jain, Aditya Golatkar, Yusheng Xie, Alessandro Achille, Ashwin Swaminathan, and Stefano Soatto. Diffusion soup: Model merging for text-to-image diffusion models. *arXiv preprint arXiv:2406.08431*, 2024.

Avishek Joey Bose, Tara Akhound-Sadegh, Guillaume Huguet, Killian Fatras, Jarrid Rector-Brooks, Cheng-Hao Liu, Andrei Cristian Nica, Maksym Korablyov, Michael Bronstein, and Alexander Tong. Se(3)-stochastic flow matching for protein backbone generation. In *The International Conference on Learning Representations (ICLR)*, 2024.

Arwen Bradley and Preetum Nakkiran. Classifier-free guidance is a predictor-corrector. *arXiv preprint arXiv:2408.09000*, 2024.

Tim Brooks, Bill Peebles, Connor Holmes, Will DePue, Yufei Guo, Li Jing, David Schnurr, Joe Taylor, Troy Luhman, Eric Luhman, Clarence Ng, Ricky Wang, and Aditya Ramesh. Video generation models as world simulators. 2024. URL https://openai.com/research/video-generation-models-as-world-simulators.

Sébastien Bubeck, Varun Chandrasekaran, Ronen Eldan, Johannes Gehrke, Eric Horvitz, Ece Kamar, Peter Lee, Yin Tat Lee, Yuanzhi Li, Scott Lundberg, et al. Sparks of artificial general intelligence: Early experiments with gpt-4. *arXiv preprint arXiv:2303.12712*, 2023.

Andrew Campbell, Jason Yim, Regina Barzilay, Tom Rainforth, and Tommi Jaakkola. Generative flows on discrete state-spaces: Enabling multimodal flows with applications to protein co-design. *arXiv preprint arXiv:2402.04997*, 2024.

Tri Dao, Dan Fu, Stefano Ermon, Atri Rudra, and Christopher Ré. Flashattention: Fast and memory-efficient exact attention with io-awareness. *Advances in Neural Information Processing Systems*, 35:16344–16359, 2022.

Justas Dauparas, Ivan Anishchenko, Nathaniel Bennett, Hua Bai, Robert J Ragotte, Lukas F Milles, Basile IM Wicky, Alexis Courbet, Rob J de Haas, Neville Bethel, et al. Robust deep learning–based protein sequence design using proteinmpnn. *Science*, 378(6615):49–56, 2022.

Prafulla Dhariwal and Alexander Nichol. Diffusion models beat gans on image synthesis. *Advances in neural information processing systems*, 34:8780–8794, 2021.

Q. Dong, Lei L. Li, D. Dai, C. Zheng, Z. Wu, B. Chang, X. Sun, J. Xu, and Z. Sui. A survey for in-context learning. *arXiv preprint arXiv:2301.00234*, 2022.

Yilun Du and Leslie Kaelbling. Compositional generative modeling: A single model is not all you need. *arXiv preprint arXiv:2402.01103*, 2024.

Yilun Du, Shuang Li, and Igor Mordatch. Compositional visual generation with energy based models. *Advances in Neural Information Processing Systems*, 33:6637–6647, 2020.

Yilun Du, Conor Durkan, Robin Strudel, Joshua B Tenenbaum, Sander Dieleman, Rob Fergus, Jascha Sohl-Dickstein, Arnaud Doucet, and Will Sussman Grathwohl. Reduce, reuse, recycle: Compositional generation with energy-based diffusion models and mcmc. In *International conference on machine learning*, pp. 8489–8510. PMLR, 2023.

Nouha Dziri, Ximing Lu, Melanie Sclar, Xiang Lorraine Li, Liwei Jiang, Bill Yuchen Lin, Sean Welleck, Peter West, Chandra Bhagavatula, Ronan Le Bras, et al. Faith and fate: Limits of transformers on compositionality. *Advances in Neural Information Processing Systems*, 36, 2024.

Aditya Golatkar, Alessandro Achille, Ashwin Swaminathan, and Stefano Soatto. Training data protection with compositional diffusion models. *arXiv preprint arXiv:2308.01937*, 2023.

A Herbert and M Sternberg. Maxcluster: A tool for protein structure comparison and clustering, 2008.

Geoffrey E Hinton. Training products of experts by minimizing contrastive divergence. *Neural computation*, 14(8):1771–1800, 2002.

Jonathan Ho and Tim Salimans. Classifier-free diffusion guidance. *arXiv preprint arXiv:2207.12598*, 2022.

Jonathan Ho, Ajay Jain, and Pieter Abbeel. Denoising diffusion probabilistic models. *Advances in Neural Information Processing Systems*, 33:6840–6851, 2020.

Yushi Hu, Benlin Liu, Jungo Kasai, Yizhong Wang, Mari Ostendorf, Ranjay Krishna, and Noah A. Smith. Tifa: Accurate and interpretable text-to-image faithfulness evaluation with question answering. In *Proceedings of the IEEE/CVF International Conference on Computer Vision (ICCV)*, pp. 20406–20417, October 2023.

Guillaume Huguet, James Vuckovic, Kilian Fatras, Eric Thibodeau-Laufer, Pablo Lemos, Riashat Islam, Cheng-Hao Liu, Jarrid Rector-Brooks, Tara Akhound-Sadegh, Michael Bronstein, et al. Sequence-augmented se (3)-flow matching for conditional protein backbone generation. *arXiv preprint arXiv:2405.20313*, 2024.

Michael F Hutchinson. A stochastic estimator of the trace of the influence matrix for laplacian smoothing splines. *Communications in Statistics-Simulation and Computation*, 18(3):1059–1076, 1989.

John B Ingraham, Max Baranov, Zak Costello, Karl W Barber, Wujie Wang, Ahmed Ismail, Vincent Frappier, Dana M Lord, Christopher Ng-Thow-Hing, Erik R Van Vlack, et al. Illuminating protein space with a programmable generative model. *Nature*, 623(7989):1070–1078, 2023.

Marco Jiralerspong, Avishek Joey Bose, Ian Gemp, Chongli Qin, Yoram Bachrach, and Gauthier Gidel. Feature likelihood score: Evaluating generalization of generative models using samples, 2023.

Jared Kaplan, Sam McCandlish, Tom Henighan, Tom B Brown, Benjamin Chess, Rewon Child, Scott Gray, Alec Radford, Jeffrey Wu, and Dario Amodei. Scaling laws for neural language models. *arXiv preprint arXiv:2001.08361*, 2020.

Lingkai Kong, Yuanqi Du, Wenhao Mu, Kirill Neklyudov, Valentin De Bortol, Haorui Wang, Dongxia Wu, Aaron Ferber, Yi-An Ma, Carla P Gomes, et al. Diffusion models as constrained samplers for optimization with unknown constraints. *arXiv preprint arXiv:2402.18012*, 2024.

Woosuk Kwon, Zhuohan Li, Siyuan Zhuang, Ying Sheng, Lianmin Zheng, Cody Hao Yu, Joseph Gonzalez, Hao Zhang, and Ion Stoica. Efficient memory management for large language model serving with pagedattention. In *Proceedings of the 29th Symposium on Operating Systems Principles*, pp. 611–626, 2023.

Yeqing Lin, Minji Lee, Zhao Zhang, and Mohammed AlQuraishi. Out of many, one: Designing and scaffolding proteins at the scale of the structural universe with genie 2. *arXiv preprint arXiv:2405.15489*, 2024.

Zeming Lin, Halil Akin, Roshan Rao, Brian Hie, Zhongkai Zhu, Wenting Lu, Nikita Smetanin, Allan dos Santos Costa, Maryam Fazel-Zarandi, Tom Sercu, Sal Candido, et al. Language models of protein sequences at the scale of evolution enable accurate structure prediction. *bioRxiv*, 2022.

Yaron Lipman, Ricky TQ Chen, Heli Ben-Hamu, Maximilian Nickel, and Matt Le. Flow matching for generative modeling. *International Conference on Learning Representations*, 2022.

Sidney Lyayuga Lisanza, Jake Merle Gershon, Sam Tipps, Lucas Arnoldt, Samuel Hendel, Jeremiah Nelson Sims, Xinting Li, and David Baker. Joint generation of protein sequence and structure with rosettafold sequence space diffusion. *bioRxiv*, pp. 2023–05, 2023.

Nan Liu, Shuang Li, Yilun Du, Antonio Torralba, and Joshua B Tenenbaum. Compositional visual generation with composable diffusion models. In *European Conference on Computer Vision*, pp. 423–439. Springer, 2022a.

Qiang Liu. Rectified flow: A marginal preserving approach to optimal transport. *arXiv preprint arXiv:2209.14577*, 2022.

Xingchao Liu, Chengyue Gong, and Qiang Liu. Flow straight and fast: Learning to generate and transfer data with rectified flow. *International Conference on Learning Representations*, 2022b.

Michael Luo, Justin Wong, Brandon Trabucco, Yanping Huang, Joseph E. Gonzalez, Zhifeng Chen, Ruslan Salakhutdinov, and Ion Stoica. Stylus: Automatic adapter selection for diffusion models. *Advances in Neural Information Processing Systems*, 2024.

Leland McInnes, John Healy, and James Melville. Umap: Uniform manifold approximation and projection for dimension reduction, 2018.

Midjourney. https://www.midjourney.com/home/, 2023. Accessed: 2023-09-09.

Weili Nie, Arash Vahdat, and Anima Anandkumar. Controllable and compositional generation with latent-space energy-based models. *Advances in Neural Information Processing Systems*, 34: 13497–13510, 2021.

Bernt Øksendal. Stochastic differential equations. In *Stochastic differential equations*, pp. 65–84. Springer, 2003.

OpenAI. Gpt-4 technical report. *ArXiv*, abs/2303.08774, 2023.

Alec Radford, Jong Wook Kim, Chris Hallacy, Aditya Ramesh, Gabriel Goh, Sandhini Agarwal, Girish Sastry, Amanda Askell, Pamela Mishkin, Jack Clark, et al. Learning transferable visual models from natural language supervision. In *International conference on machine learning*, pp. 8748–8763. PMLR, 2021.

Aditya Ramesh, Mikhail Pavlov, Gabriel Goh, Scott Gray, Chelsea Voss, Alec Radford, Mark Chen, and Ilya Sutskever. Zero-shot text-to-image generation. In *International Conference on Machine Learning*. PMLR, 2021.

Milong Ren, Tian Zhu, and Haicang Zhang. Carbonnovo: Joint design of protein structure and sequence using a unified energy-based model. In *Forty-first International Conference on Machine Learning*, 2024.

Robin Rombach, Andreas Blattmann, Dominik Lorenz, Patrick Esser, and Björn Ommer. High-resolution image synthesis with latent diffusion models. In *Proceedings of the IEEE/CVF Conference on Computer Vision and Pattern Recognition (CVPR)*, pp. 10684–10695, June 2022.

Rylan Schaeffer, Brando Miranda, and Sanmi Koyejo. Are emergent abilities of large language models a mirage? arxiv. *arXiv preprint arXiv:2304.15004*, 2023.

Christoph Schuhmann, Romain Beaumont, Richard Vencu, Cade Gordon, Ross Wightman, Mehdi Cherti, Theo Coombes, Aarush Katta, Clayton Mullis, Mitchell Wortsman, et al. LAION-5B: An open large-scale dataset for training next generation image-text models. *Advances in Neural Information Processing Systems*, 2022.

Yang Song, Jascha Sohl-Dickstein, Diederik P Kingma, Abhishek Kumar, Stefano Ermon, and Ben Poole. Score-based generative modeling through stochastic differential equations. In *International Conference on Learning Representations*, 2020.

Stability AI. https://stability.ai/stablediffusion, 2023. Accessed: 2023-09-09.

Jacob Steinhardt. AI Forecasting: One Year In . https://bounded-regret.ghost.io/ai-forecasting-one-year-in/, 2022. Accessed: 2023-09-09.

Trieu H Trinh, Yuhuai Wu, Quoc V Le, He He, and Thang Luong. Solving olympiad geometry without human demonstrations. *Nature*, 625(7995):476–482, 2024.

Brian L. Trippe, Jason Yim, Doug Tischer, David Baker, Tamara Broderick, Regina Barzilay, and Tommi S. Jaakkola. Diffusion probabilistic modeling of protein backbones in 3d for the motif-scaffolding problem. In *The Eleventh International Conference on Learning Representations*, 2023. URL https://openreview.net/forum?id=6TxBxqNME1Y.

Michel Van Kempen, Stephanie S Kim, Charlotte Tumescheit, Milot Mirdita, Jeongjae Lee, Cameron LM Gilchrist, Johannes Söding, and Martin Steinegger. Fast and accurate protein structure search with foldseek. *Nature biotechnology*, 42(2):243–246, 2024.

Pascal Vincent. A connection between score matching and denoising autoencoders. *Neural computation*, 23(7):1661–1674, 2011.

Chentong Wang, Yannan Qu, Zhangzhi Peng, Yukai Wang, Hongli Zhu, Dachuan Chen, and Longxing Cao. Proteus: exploring protein structure generation for enhanced designability and efficiency. *bioRxiv*, pp. 2024–02, 2024.

Joseph L. Watson, David Juergens, Nathaniel R. Bennett, Brian L. Trippe, Jason Yim, Helen E. Eisenach, Woody Ahern, Andrew J. Borst, Robert J. Ragotte, Lukas F. Milles, Basile I. M. Wicky, Nikita Hanikel, Samuel J. Pellock, Alexis Courbet, William Sheffler, Jue Wang, Preetham Venkatesh, Isaac Sappington, Susana Vázquez Torres, Anna Lauko, Valentin De Bortoli, Emile Mathieu, Sergey Ovchinnikov, Regina Barzilay, Tommi S. Jaakkola, Frank DiMaio, Minkyung Baek, and David Baker. De novo design of protein structure and function with rfdiffusion. *Nature*, 620(7976):1089–1100, 2023. ISSN 1476-4687.

Jiazheng Xu, Xiao Liu, Yuchen Wu, Yuxuan Tong, Qinkai Li, Ming Ding, Jie Tang, and Yuxiao Dong. Imagereward: Learning and evaluating human preferences for text-to-image generation. *Advances in Neural Information Processing Systems*, 36, 2024.

Jason Yim, Andrew Campbell, Andrew Y. K. Foong, Michael Gastegger, José Jiménez-Luna, Sarah Lewis, Victor Garcia Satorras, Bastiaan S. Veeling, Regina Barzilay, Tommi Jaakkola, and Frank Noé. Fast protein backbone generation with se(3) flow matching, 2023a.

Jason Yim, Brian L Trippe, Valentin De Bortoli, Emile Mathieu, Arnaud Doucet, Regina Barzilay, and Tommi Jaakkola. Se (3) diffusion model with application to protein backbone generation. *arXiv preprint arXiv:2302.02277*, 2023b.

Jason Yim, Andrew Campbell, Emile Mathieu, Andrew YK Foong, Michael Gastegger, José Jiménez-Luna, Sarah Lewis, Victor Garcia Satorras, Bastiaan S Veeling, Frank Noé, et al. Improved motif-scaffolding with se (3) flow matching. *arXiv preprint arXiv:2401.04082*, 2024.

Ming Zhong, Yelong Shen, Shuohang Wang, Yadong Lu, Yizhu Jiao, Siru Ouyang, Donghan Yu, Jiawei Han, and Weizhu Chen. Multi-lora composition for image generation. *arXiv preprint arXiv:2402.16843*, 2024.

APPENDIX

A PROOFS FOR SEC. 2

A.1 PROOF OF PROP. 1

Proposition 1. [Reverse-time SDEs/ODE] *Marginal densities $q_t(x)$ induced by Eq. (1) correspond to the densities induced by the following SDE that goes back in time ($\tau = 1 - t$) with the corresponding initial condition*

$$dx_\tau = \left(-f_t(x_\tau) + \left(\frac{g_t^2}{2} + \xi_\tau\right)\nabla \log q_t(x_\tau)\right)d\tau + \sqrt{2\xi_\tau}d\overline{W}_\tau\,, \quad x_{\tau=0} \sim q_1(x_0)\,, \tag{2}$$

where $\overline{W}_\tau$ is the standard Wiener process in time τ, and ξ_τ is any positive schedule.

For the forward SDE we can write the corresponding Fokker-Planck equation

$$\frac{\partial}{\partial t}q_t(x) = -\big\langle \nabla, q_t(x)f_t(x)\big\rangle + \frac{g_t^2}{2}\Delta q_t(x)\,, \tag{19}$$

then for the inverse time $\tau = 1 - t$, we have

$$\frac{\partial}{\partial \tau}q_{1-\tau}(x) = \big\langle \nabla, q_{1-\tau}(x)f_{1-\tau}(x)\big\rangle - \frac{g_{1-\tau}^2}{2}\Delta q_{1-\tau}(x) \tag{20}$$

$$= \left\langle \nabla, q_{1-\tau}(x)\left(f_{1-\tau}(x) - \frac{g_{1-\tau}^2}{2}\nabla \log q_{1-\tau}(x)\right)\right\rangle \tag{21}$$

$$= -\left\langle \nabla, q_{1-\tau}(x)\left(-f_{1-\tau}(x) + \left(\frac{g_{1-\tau}^2}{2} + \xi_\tau\right)\nabla \log q_{1-\tau}(x)\right)\right\rangle + \xi_\tau \Delta q_{1-\tau}(x)\,, \tag{22}$$

which corresponds to the SDE

$$dx_\tau = d\tau\left(-f_{1-\tau}(x_\tau) + \left(\frac{g_{1-\tau}^2}{2} + \xi_\tau\right)\nabla \log q_{1-\tau}(x_\tau)\right) + \sqrt{2\xi_\tau}d\overline{W}_\tau\,. \tag{23}$$

A.2 PROOF OF PROP. 2

Proposition 2. [Ornstein–Uhlenbeck SDE] *The time-dependent densities in Eq. (3) correspond to the marginal densities of the following SDE, with the corresponding initial condition*

$$dx_t = \underbrace{\frac{\partial \log \alpha_t}{\partial t}x_t}_{f_t(x_t)}\,dt + \underbrace{\sqrt{2\sigma_t^2\frac{\partial}{\partial t}\log\frac{\sigma_t}{\alpha_t}}}_{g_t}\,dW_t\,, \quad x_0 \sim q_0(x_0)\,. \tag{4}$$

Proof. For individual components q_t^i from Eq. (3), we have to find the vector field satisfying the continuity equation, which we can rewrite as

$$\frac{\partial}{\partial t}\log q_t^i(x) = -\big\langle \nabla_x, v_t^i(x)\big\rangle - \big\langle \nabla_x \log q_t^i(x), v_t^i(x)\big\rangle\,. \tag{24}$$

Using the formula for the density of the normal distribution $q_t^i(x) = \mathcal{N}(x \,|\, \alpha_t\mu^i, \sigma_t^2)$, we have

$$\nabla_x \log q_t^i(x) = -\frac{1}{\sigma_t^2}(x - \alpha_t\mu^i)\,, \tag{25}$$

$$\frac{\partial}{\partial t}\log q_t^i(x) = d\frac{\partial}{\partial t}\log\sigma_t + \frac{1}{\sigma_t^3}\frac{\partial \sigma_t}{\partial t}\big\|x - \alpha_t\mu^i\big\|^2 + \frac{1}{\sigma_t^2}\big\langle x - \alpha_t\mu^i, \mu^i\big\rangle\frac{\partial \alpha_t}{\partial t} \tag{26}$$

$$= \left\langle \nabla_x, \frac{\partial \log\sigma_t}{\partial t}x\right\rangle - \left\langle \nabla_x \log q_t^i(x), \underbrace{\frac{\partial \log\sigma_t}{\partial t}(x - \alpha_t\mu^i) + \frac{\partial \alpha_t}{\partial t}\mu^i}_{v_t^i(x)}\right\rangle \tag{27}$$

$$= \big\langle \nabla_x, v_t^i(x)\big\rangle - \big\langle \nabla_x \log q_t^i(x), v_t^i(x)\big\rangle\,. \tag{28}$$

For the mixture of densities q_t from Eq. (3), we can use Prop. 3 and write

$$v_t(x) = \frac{1}{q_t(x)N}\sum_{i=1}^{N} q_t^i(x)\left[\frac{\partial \log \sigma_t}{\partial t}(x - \alpha_t \mu^i) + \frac{\partial \alpha_t}{\partial t}\mu^i\right] \tag{29}$$

$$= \frac{\partial \log \sigma_t}{\partial t}x + \left[\frac{\partial \alpha_t}{\partial t} - \frac{\partial \log \sigma_t}{\partial t}\alpha_t\right]\frac{1}{q_t(x)N}\sum_{i=1}^{N} q_t^i(x)\mu^i\,. \tag{30}$$

At the same time

$$\nabla_x \log q_t(x) = \frac{1}{q_t(x)N}\sum_{i=1}^{N} q_t^i(x)\left[-\frac{1}{\sigma_t^2}(x - \alpha_t\mu^i)\right], \tag{31}$$

$$\frac{1}{q_t(x)N}\sum_{i=1}^{N} q_t^i(x)\mu^i = \frac{1}{\alpha_t}\left[\sigma_t^2 \nabla_x \log q_t(x) + x\right]. \tag{32}$$

Using this formula in Eq. (30), we have

$$v_t(x) = \left[\frac{\partial \log \sigma_t}{\partial t} + \frac{1}{\alpha_t}\frac{\partial \alpha_t}{\partial t} - \frac{\partial \log \sigma_t}{\partial t}\right]x + \left[\frac{\partial \alpha_t}{\partial t} - \frac{\partial \log \sigma_t}{\partial t}\alpha_t\right]\frac{\sigma_t^2}{\alpha_t}\nabla_x \log q_t(x) \tag{33}$$

$$= \frac{\partial \log \alpha_t}{\partial t}x - \sigma_t^2 \frac{\partial}{\partial t}\log\frac{\sigma_t}{\alpha_t}\nabla_x \log q_t(x)\,. \tag{34}$$

Hence, we have

$$\frac{\partial}{\partial t}q_t(x) = -\left\langle \nabla, q_t(x)v_t(x)\right\rangle = -\left\langle \nabla, q_t(x)\left(\frac{\partial \log \alpha_t}{\partial t}x\right)\right\rangle + \sigma_t^2\frac{\partial}{\partial t}\log\frac{\sigma_t}{\alpha_t}\Delta q_t(x)\,, \tag{35}$$

which corresponds to the SDE in the statement. □

A.3 Proof of Prop. 3

Proposition 3. [Superposition of ODEs (Liu, 2022)] *The mixture density in Eq. (6) follows the continuity equation with the superposed vector fields from Eq. (5), i.e.*

$$\frac{\partial}{\partial t}q_t^{\text{mix}}(x) = -\left\langle \nabla_x, q_t^{\text{mix}}(x)v_t(x)\right\rangle, \quad v_t(x) = \frac{1}{\sum_{j=1}^{N}\omega^j q_t^j(x)}\sum_{i=1}^{N}\omega^i q_t^i(x)v_t^i(x)\,. \tag{7}$$

Proof. By the straightforward substitution, we have

$$\frac{\partial}{\partial t}q_t^{\text{mix}}(x) = \sum_{i=1}^{m}\omega^i\frac{\partial}{\partial t}q_t^i(x) = -\sum_{i=1}^{m}\omega^i\left\langle \nabla_x, q_t^i(x)v_t^i(x)\right\rangle \tag{36}$$

$$= -\left\langle \nabla_x, \sum_{i=1}^{m}\omega^i q_t^i(x)v_t^i(x)\right\rangle = -\left\langle \nabla_x, \frac{q_t^{\text{mix}}(x)}{q_t^{\text{mix}}(x)}\sum_{i=1}^{m}\omega^i q_t^i(x)v_t^i(x)\right\rangle \tag{37}$$

$$= -\left\langle \nabla_x, q_t^{\text{mix}}(x)\underbrace{\frac{1}{\sum_{j=1}^{m}\omega^j q_t^j(x)}\sum_{i=1}^{m}\omega^i q_t^i(x)v_t^i(x)}_{v_t(x)}\right\rangle. \tag{38}$$

□

A.4 Proof of Prop. 4

Proposition 4. [Superposition of SDEs] *The mixture $q_t^{\text{mix}}(x) := \sum_{i=1}^{N}\omega^i q_t^i(x)$ of density marginals $\{q_t^i(x)\}_{i=1}^{N}$ induced by SDEs from Eq. (8) corresponds to the following SDE*

$$dx_\tau = u_\tau(x_\tau)d\tau + g_\tau d\overline{W}_\tau\,, \quad u_t(x) = \frac{1}{\sum_{j=1}^{N}\omega^j q_t^j(x)}\sum_{i=1}^{N}\omega^i q_t^i(x)u_t^i(x)\,. \tag{9}$$

Proof. By the straightforward substitution, we have

$$\frac{\partial}{\partial t} q_t^{\text{mix}}(x) = \sum_{i=1}^{m} \omega^i \frac{\partial}{\partial t} q_t^i(x) = \sum_{i=1}^{m} \omega^i \left(-\langle \nabla_x, q_t^i(x) u_t^i(x) \rangle + \frac{g_t^2}{2} \Delta q_t^i(x) \right). \tag{39}$$

The first term is analogous to Prop. 3, i.e.

$$\sum_{i=1}^{m} \omega^i \left(-\langle \nabla_x, q_t^i(x) u_t^i(x) \rangle \right) = -\left\langle \nabla_x, q_t^{\text{mix}}(x) \underbrace{\frac{1}{\sum_{j=1}^{m} \omega^j q_t^j(x)} \sum_{i=1}^{m} \omega^i q_t^i(x) u_t^i(x)}_{u_t(x)} \right\rangle. \tag{40}$$

The second term is

$$\sum_{i=1}^{m} \omega^i \frac{g_t^2}{2} \Delta q_t^i(x) = \frac{g_t^2}{2} \Delta \sum_{i=1}^{m} \omega^i \Delta q_t^i(x) = \frac{g_t^2}{2} \Delta q_t^{\text{mix}}(x). \tag{41}$$

This results in the following PDE

$$\frac{\partial}{\partial t} q_t^{\text{mix}}(x) = -\left\langle \nabla_x, q_t^{\text{mix}}(x) \underbrace{\frac{1}{\sum_{j=1}^{m} \omega^j q_t^j(x)} \sum_{i=1}^{m} \omega^i q_t^i(x) u_t^i(x)}_{u_t(x)} \right\rangle + \frac{g_t^2}{2} \Delta q_t^{\text{mix}}(x). \tag{42}$$

□

B Flows and Diffusion as a Superposition of Elementary Vector Fields

From Prop. 3, one can immediately get the main principle for the simulation-free training of generative flow models, as demonstrated in the following proposition.

Proposition 7. [Superposition of L_2-losses] *For the parametric vector field model $v_t(x;\theta)$ with parameters θ, the L_2-loss for the vector field from Prop. 3 can be decomposed into the losses for the vector fields from Eq. (5), i.e.*

$$\int_0^1 dt\, \mathbb{E}_{q_t^{\text{mix}}(x)} \|v_t(x) - v_t(x;\theta)\|^2 = \sum_{i=1}^{N} \omega_i \int_0^1 dt\, \mathbb{E}_{q_t^i(x)} \left\|v_t^i(x) - v_t(x;\theta)\right\|^2 + \text{constant},$$

where the constant does not depend on the parameters θ.

Proof. By the straightforward calculation, we have

$$\int_0^1 dt\, \mathbb{E}_{q_t^{\text{mix}}(x)} \|v_t(x) - v_t(x;\theta)\|^2 = \int_0^1 dt\, \mathbb{E}_{q_t^{\text{mix}}(x)} \left[\|v_t(x)\|^2 - 2\langle v_t(x), v_t(x;\theta) \rangle + \|v_t(x;\theta)\|^2 \right],$$

where the first term is constant w.r.t. θ and the last term is amenable for a straightforward estimation. The middle term, according to Prop. 3, is

$$\int dx\, q_t^{\text{mix}}(x) \langle v_t(x), v_t(x;\theta) \rangle = \int dx \sum_{i=1}^{m} \omega^i q_t^i(x) \langle v_t^i(x), v_t(x;\theta) \rangle. \tag{43}$$

Thus, we have

$$\int_0^1 dt\ \mathbb{E}_{q_t^{\text{mix}}(x)} \left[\|v_t(x)\|^2 - 2\langle v_t(x), v_t(x;\theta) \rangle + \|v_t(x;\theta)\|^2 \right] \tag{44}$$

$$= \int_0^1 dt\ \Bigg[\underbrace{\mathbb{E}_{q_t^{\text{mix}}(x)} \|v_t(x)\|^2 - \sum_{i=1}^{m} \omega^i \mathbb{E}_{q_t^i(x)} \left\|v_t^i(x)\right\|^2}_{\text{constant}} + \sum_{i=1}^{m} \omega^i \mathbb{E}_{q_t^i(x)} \left\|v_t^i(x)\right\|^2 - \tag{45}$$

$$- 2 \sum_{i=1}^{m} \omega^i \mathbb{E}_{q_t^i(x)} \langle v_t^i(x), v_t(x;\theta) \rangle + \sum_{i=1}^{m} \omega^i \mathbb{E}_{q_t^i(x)} \|v_t(x;\theta)\|^2 \Bigg] \tag{46}$$

$$= \int_0^1 dt \sum_{i=1}^m \omega^i \mathbb{E}_{q_t^i(x)} \left\| v_t^i(x) - v_t(x;\theta) \right\|^2 + \text{constant}\,. \tag{47}$$

□

The proof for proposition follows a simple extension of Liu (2022). Consequently, the generative modeling problem explicitly boils down to learning a time-dependent vector field $v_t(x, \theta)$. Moreover, for the generative modeling task, the noising process is required to satisfy the following boundary conditions $q_0^i(x) = \delta(x - \mu^i)$ and $q_1^i(x) = p_{\text{noise}}(x)\,, \forall\, i \in \mathcal{D}$. Generating samples that resemble $p_{\text{data}}(\mu)$ during inference then simply amounts to solving the reverse-time ODE with the learned model $v_t(x;\theta)$ starting from a noisy sample $x_1 \sim p_{\text{noise}}(x)$.

Diffusion models can be incorporated into the flow-based framework by selecting a Gaussian forward process which gives the marginal density at a timestep t as the mixture of corresponding Gaussians,

$$q_t^i(x) = \mathcal{N}(x \,|\, \alpha_t \mu^i, \sigma_t^2)\,, \quad q_t(x) = \frac{1}{N} \sum_{i=1}^N q_t^i(x)\,. \tag{48}$$

Under this Gaussian diffusion framework, we can express the vector fields analytically using the score, which is formalized by the following proposition.

Proposition 8. [Diffusion processes] *The time-dependent densities in Eq. (48) satisfy the following continuity equations*

$$\frac{\partial}{\partial t} q_t^i(x) = -\left\langle \nabla_x, q_t^i(x) v_t^i(x) \right\rangle, \quad v_t^i(x) = \frac{\partial \log \sigma_t}{\partial t}(x - \alpha_t \mu^i) + \frac{\partial \alpha_t}{\partial t}\mu^i\,, \tag{49}$$

$$\frac{\partial}{\partial t} q_t(x) = -\left\langle \nabla_x, q_t(x) v_t(x) \right\rangle, \quad v_t(x) = \frac{\partial \log \alpha_t}{\partial t} x - \left(\sigma_t^2 \frac{\partial}{\partial t} \log \frac{\sigma_t}{\alpha_t} \right) \nabla_x \log q_t(x)\,. \tag{50}$$

The proof repeats the proof for Prop. 2 in App. A.2 since Eq. (50) corresponds to the Ornstein-Uhlenbeck process:

$$dx_t = \frac{\partial \log \alpha_t}{\partial t} x_t dt + \sqrt{2 \left(\sigma_t^2 \frac{\partial}{\partial t} \log \frac{\sigma_t}{\alpha_t} \right)} dW_t. \tag{51}$$

Diffusion models using a Gaussian perturbation kernel enjoy the benefit of giving an exact expression for the Stein score of the perturbed data which leads to the celebrated denoising score matching objective (Vincent, 2011; Ho et al., 2020). Analogously to Prop. 7 we can write the denoising score matching objective as the superposition of the scores as demonstrated in the following proposition.

Proposition 9. [Denoising Score Matching (Vincent, 2011)] *For the parametric score model $\nabla \log q_t(x;\theta)$ with parameters θ, the score matching objective can be decomposed into the corresponding objectives for the individual scores, i.e.*

$$\int_0^1 dt \;\; \mathbb{E}_{q_t(x)} \| \nabla \log q_t(x) - \nabla \log q_t(x;\theta) \|^2 =$$

$$= \frac{1}{N} \sum_{i=1}^N \int_0^1 dt \;\; \mathbb{E}_{q_t^i(x)} \left\| \nabla \log q_t^i(x) - \nabla \log q_t(x;\theta) \right\|^2 + \text{constant}\,,$$

where the constant does not depend on the parameters θ and $\nabla \log q_t^i(x) = -\frac{1}{\sigma_t^2}(x - \alpha_t \mu^i)$.

Proof. From Prop. 8, we have

$$v_t^i(x) = \frac{\partial \log \sigma_t}{\partial t}(x - \alpha_t \mu^i) + \frac{\partial \alpha_t}{\partial t}\mu^i \tag{52}$$

$$= \frac{\partial \log \sigma_t}{\partial t}(x - (x + \sigma_t^2 \nabla \log q_t^i(x))) + \frac{\partial \alpha_t}{\partial t} \frac{1}{\alpha_t}(x + \sigma_t^2 \nabla \log q_t^i(x)) \tag{53}$$

$$= \frac{\partial \log \alpha_t}{\partial t} x + \sigma_t^2 \frac{\partial}{\partial t} \log \frac{\alpha_t}{\sigma_t} \nabla_x \log q_t^i(x) \tag{54}$$

$$v_t(x) = \frac{\partial \log \alpha_t}{\partial t} x + \sigma_t^2 \frac{\partial}{\partial t} \log \frac{\alpha_t}{\sigma_t} \nabla_x \log q_t(x) \,. \tag{55}$$

Applying the same change of variables to the parametric model

$$v_t(x;\theta) = \frac{\partial \log \alpha_t}{\partial t} x + \sigma_t^2 \frac{\partial}{\partial t} \log \frac{\alpha_t}{\sigma_t} \nabla_x \log q_t(x;\theta) \,, \tag{56}$$

and using Prop. 7, we have

$$\int_0^1 dt \;\; \mathbb{E}_{q_t(x)} \|v_t(x) - v_t(x;\theta)\|^2 = \sum_{i=1}^m \frac{1}{N} \int_0^1 dt \; \mathbb{E}_{q_t^i(x)} \left\| v_t^i(x) - v_t(x;\theta) \right\|^2 + \text{constant} \,, \tag{57}$$

$$\int_0^1 dt \;\; \mathbb{E}_{q_t(x)} \|\nabla_x \log q_t(x) - \nabla_x \log q_t(x;\theta)\|^2 \tag{58}$$

$$= \sum_{i=1}^m \frac{1}{N} \int_0^1 dt \; \mathbb{E}_{q_t^i(x)} \left\| \nabla_x \log q_t^i(x) - \nabla_x \log q_t(x;\theta) \right\|^2 + \frac{\text{constant}}{\left(\sigma_t^2 \frac{\partial}{\partial t} \log \frac{\alpha_t}{\sigma_t}\right)} \,, \tag{59}$$

which concludes the proof. □

C Density Estimators

Proposition 5. [Smooth density estimator] *For the integral curve $x(t)$ solving $dx/dt = u_t(x_t)$, and the density $q_t^i(x(t))$ satisfying the continuity equation $\frac{\partial}{\partial t} q_t^i(x) = -\langle \nabla_x, q_t^i(x) v_t^i(x) \rangle$, the log-density along the curve changes according to the following ODE*

$$\frac{d}{dt} \log q_t^i(x(t)) = -\langle \nabla_x, v_t^i(x) \rangle - \langle \nabla_x \log q_t^i(x), v_t^i(x) - u_t(x) \rangle \,. \tag{10}$$

Proof. By straightforward computation, we have

$$\frac{d}{dt} \log q_t^i(x(t)) = \frac{\partial}{\partial t} \log q_t^i(x) + \left\langle \nabla_x \log q_t^i(x), \frac{dx}{dt} \right\rangle \,, \tag{60}$$

and using the continuity equation $\frac{\partial}{\partial t} q_t^i(x) = -\langle \nabla_x, q_t^i(x) v_t^i(x) \rangle$, we have

$$\frac{\partial}{\partial t} \log q_t^i(x) = -\langle \nabla_x, v_t^i(x) \rangle - \langle \nabla_x \log q_t^i(x), v_t^i(x) \rangle \,, \tag{61}$$

$$\frac{d}{dt} \log q_t^i(x(t)) = -\langle \nabla_x, v_t^i(x) \rangle - \langle \nabla_x \log q_t^i(x), v_t^i(x) - u_t(x) \rangle \,. \tag{62}$$

□

Theorem 1. [Ôti density estimator] *Consider time-dependent density $q_t(x)$ induced by the marginals of the following "forward" process*

$$dx_t = f_t(x_t)dt + g_t dW_t \,, \quad x_{t=0} \sim q_0(x) \,, \quad t \in [0,1] \,, \tag{11}$$

where dW_t is the Wiener process. Then, for the following "backward" SDE (with $\tau = 1 - t$)

$$dx_\tau = u_\tau(x_\tau)d\tau + g_{1-\tau} d\overline{W}_\tau \,, \quad \tau \in [0,1] \,, \tag{12}$$

the change of the log-density $\log q_\tau(x_\tau)$ follows the following SDE

$$\begin{aligned} d \log q_{1-\tau}(x_\tau) = \langle dx_\tau, \nabla \log q_{1-\tau}(x_\tau) \rangle + \Big(\langle \nabla, f_{1-\tau}(x_\tau) \rangle + \\ + \left\langle f_{1-\tau}(x_\tau) - \frac{g_{1-\tau}^2}{2} \nabla \log q_{1-\tau}(x_\tau), \nabla \log q_{1-\tau}(x_\tau) \right\rangle \Big) d\tau \,. \end{aligned} \tag{13}$$

Proof. The Fokker-Planck equation describing the evolution of the marginals for the forward process is

$$\frac{\partial q_t(x)}{\partial t} = -\langle \nabla, f_t(x) q_t(x) \rangle + \frac{g_t^2}{2} \Delta q_t(x) \,, \tag{63}$$

hence, for the inverse time $\tau = 1 - t$, we have

$$\frac{\partial}{\partial \tau} q_{1-\tau}(x) = \langle \nabla, f_{1-\tau}(x) q_{1-\tau}(x) \rangle - \frac{g_{1-\tau}^2}{2} \Delta q_{1-\tau}(x) \tag{64}$$

$$\begin{aligned} \frac{\partial}{\partial \tau} \log q_{1-\tau}(x) = \langle \nabla, f_{1-\tau}(x) \rangle + \langle \nabla \log q_{1-\tau}(x), f_{1-\tau}(x) \rangle - \\ - \frac{g_{1-\tau}^2}{2} \Delta \log p_{1-\tau}(x) - \frac{g_{1-\tau}^2}{2} \|\nabla \log q_{1-\tau}(x)\|^2 \,. \end{aligned} \tag{65}$$

For the following reverse-time SDE

$$dx_\tau = u_\tau(x_\tau) d\tau + g_{1-\tau} d\overline{W}_\tau \,, \tag{66}$$

using Itô's lemma for $\log q_{1-\tau}(x_\tau)$, we have

$$d \log q_{1-\tau}(x_\tau) = \Bigg(\frac{\partial}{\partial \tau} \log q_{1-\tau}(x_\tau) + \langle \nabla \log q_{1-\tau}(x_\tau), u_\tau(x_\tau) \rangle + \tag{67}$$

$$+ \frac{g_{1-\tau}^2}{2} \Delta \log q_\tau(x_\tau) \Bigg) d\tau + g_{1-\tau} \langle \nabla \log q_{1-\tau}(x_\tau), d\overline{W}_\tau \rangle \,. \tag{68}$$

Using Eq. (65), we have

$$d \log q_{1-\tau}(x_\tau) = \Bigg(\Bigg\langle \nabla \log q_{1-\tau}(x_\tau), f_{1-\tau}(x_\tau) - \frac{g_{1-\tau}^2}{2} \nabla \log q_{1-\tau}(x_\tau) \Bigg\rangle + \tag{69}$$

$$+ \langle \nabla, f_{1-\tau}(x_\tau) \rangle \Bigg) d\tau + \Bigg\langle \nabla \log q_{1-\tau}(x_\tau), \underbrace{u_\tau(x_\tau) d\tau + g_{1-\tau} d\overline{W}_\tau}_{dx_\tau} \Bigg\rangle \,. \tag{70}$$

□

C.1 Proof of Prop. 6

Proposition 6. [Density control] *For the SDE*

$$dx_\tau = \sum_{j=1}^{M} \kappa_j u_\tau^j(x_\tau) d\tau + g_{1-\tau} d\overline{W}_\tau \,, \tag{16}$$

where κ are the weights of different models and $\sum_j \kappa_j = 1$, one can find κ that satisfies

$$d \log q_{1-\tau}^i(x_\tau) = d \log q_{1-\tau}^j(x_\tau) \,, \quad \forall \;\; i, j \in [M] \,, \tag{17}$$

by solving a system of M linear equations w.r.t. κ.

Proof. Using the result of Thm. 1, for the density change of every model, we have

$$d \log q_{1-\tau}^i(x_\tau) = \langle dx_\tau, \nabla \log q_{1-\tau}^i(x_\tau) \rangle + \Bigg(\langle \nabla, f_{1-\tau}(x_\tau) \rangle + \tag{71}$$

$$+ \Bigg\langle f_{1-\tau}(x_\tau) - \frac{g_{1-\tau}^2}{2} \nabla \log q_{1-\tau}^i(x_\tau), \nabla \log q_{1-\tau}^i(x_\tau) \Bigg\rangle \Bigg) d\tau \tag{72}$$

$$= \sum_{j=1}^{M} \kappa_j d\tau \langle u_\tau^j(x_\tau), \nabla \log q_{1-\tau}^i(x_\tau) \rangle + \Bigg(\langle \nabla, f_{1-\tau}(x_\tau) \rangle + \tag{73}$$

$$+ \Bigg\langle g_{1-\tau} d\overline{W}_\tau + \Bigg(f_{1-\tau}(x_\tau) - \frac{g_{1-\tau}^2}{2} \nabla \log q_{1-\tau}^i(x_\tau) \Bigg) d\tau, \nabla \log q_{1-\tau}^i(x_\tau) \Bigg\rangle \Bigg) \,. \tag{74}$$

Let us denote

$$a_{ij} = d\tau \left\langle u^j_\tau(x_\tau), \nabla \log q^i_{1-\tau}(x_\tau) \right\rangle, \tag{75}$$

$$b_i = \left\langle \nabla, f_{1-\tau}(x_\tau) \right\rangle + \left\langle g_{1-\tau} d\overline{W}_\tau + \left(f_{1-\tau}(x_\tau) - \frac{g^2_{1-\tau}}{2} \nabla \log q^i_{1-\tau}(x_\tau) \right) d\tau, \nabla \log q^i_{1-\tau}(x_\tau) \right\rangle. \tag{76}$$

Then the change of densities can be written as the following linear transformation

$$\begin{bmatrix} d \log q^1_{1-\tau}(x_\tau) \\ \dots \\ d \log q^i_{1-\tau}(x_\tau) \\ \dots \\ d \log q^M_{1-\tau}(x_\tau) \end{bmatrix} = A\kappa + b\,. \tag{77}$$

Solving

$$A\kappa + b = \begin{bmatrix} 1 \\ \dots \\ 1 \\ \dots \\ 1 \end{bmatrix}, \tag{78}$$

and normalizing kappas so we have $\sum_j \kappa_j = 1$, we get the solution. □

D Discrete-time perspective on Thm. 1

In this section we derive Thm. 1 from another perspective by operating with discrete time transition kernels and the detailed balance. Namely, we aim to compute the marginal density by starting from the detailed balance equation, which states the equivalence of the following joint densities:

$$q_t(y) k_{\Delta t}(x \,|\, y) = q_{t+\Delta t}(x) r_{\Delta t}(y \,|\, x). \tag{79}$$

The detailed balance condition simply states the pair (x, y) can be sampled in two equivalent ways: 1.) sampling y from the marginal $q_t(y)$ and then sampling x via the noising kernel $k_{\Delta t}(x \,|\, y)$, or 2.) sampling x from $q_{t+\Delta t}(y)$ and then denoising it via $r_{\Delta t}(y \,|\, x)$. Indeed, there are infinitely many valid kernels that may satisfy the detailed balance; we make a specific choice informed by the following principle. We aim to construct a universal noising kernel that is independent of the data distribution or other densities, i.e. $p_{\text{data}}(\cdot), q_t(\cdot), q_{t+\Delta t}(\cdot)$. Remarkably, this principle results in a unique kernel choice, which we formalize in the following proposition.

Proposition 10. [Universal noising kernel] *For any data density $p_{\text{data}}(\mu)$, for the continuous noising process $q_t(x) = \int d\mu\, \mathcal{N}(x \,|\, \alpha_t \mu, \sigma_t^2) p_{\text{data}}(\mu)$, there exists unique noising kernel*

$$k_{\Delta t}(x \,|\, y) = \mathcal{N}\left(x \,\middle|\, \frac{\alpha_{t+\Delta t}}{\alpha_t} y, S^2_{t+\Delta t} \right), q_{t+\Delta t}(x) = \int dy\; k_{\Delta t}(y \,|\, x) q_t(y), \tag{80}$$

where $S^2_{t+\Delta t} = \sigma^2_{t+\Delta t} - \sigma_t^2 \frac{\alpha^2_{t+\Delta t}}{\alpha_t^2}$ and it is independent of the densities $p_{\text{data}}(\cdot), q_t(\cdot), q_{t+\Delta t}(\cdot)$.

The proof for this proposition is presented in App. D.1. Note that the proposition holds exactly for any Δt—i.e. there are no any assumptions on the scale of Δt or any approximations.

Once the noising kernel is fixed, the detailed balance Eq. (79) uniquely defines the denoising kernel $r_{\Delta t}(y \,|\, x)$ that propagates samples back in time. However, the analytic form of this kernel depends on the densities $q_{t+\Delta t}(x)$ and $q_t(y)$, which are unavailable for the modern large-scale diffusion models that are served using limited API endpoints. Therefore, we consider the Gaussian approximation of the reverse kernel and justify its applicability in the following theorem.

Theorem 2. [Denoising kernel] *For the universal noising kernel $k_{\Delta t}(x \,|\, y)$, the Gaussian approximation of the corresponding reverse kernel $r_{\Delta t}(y \,|\, x) = k_{\Delta t}(x \,|\, y) q_t(y) / q_{t+\Delta t}(x)$ is*

$$\tilde{r}_{\Delta t}(y \,|\, x) = \mathcal{N}\left(y \,\middle|\, \frac{\alpha_t}{\alpha_{t+\Delta t}} x + \frac{\alpha_t}{\alpha_{t+\Delta t}} S^2_{t+\Delta t} \nabla \log q_{t+\Delta t}(x), \left(\frac{\alpha_t}{\alpha_{t+\Delta t}} S_{t+\Delta t} \right)^2 \right), \tag{81}$$

which corresponds to a single step of the Euler discretization of the following SDE

$$dx_\tau = -\left(\frac{\partial}{\partial t}\log\alpha_t x - 2\sigma_t^2\frac{\partial}{\partial t}\log\frac{\sigma_t}{\alpha_t}\nabla_x \log q_t(x)\right)\cdot d\tau + \sqrt{2\sigma_t^2\frac{\partial}{\partial t}\log\frac{\sigma_t}{\alpha_t}}dW_\tau\,, \tag{82}$$

and

$$D_{\mathrm{KL}}(\tilde{r}_{\Delta t}(y\,|\,x)\|r_{\Delta t}(y\,|\,x)) = o(\Delta t)\,. \tag{83}$$

See proof in App. D.3. Given the noising kernel from Prop. 10 and the approximation of the reverse kernel from Thm. 2, we propose to estimate the log marginal density of the current sample using the detailed balance as follows,

$$\log q_t(y) - \log q_{t+\Delta t}(x) = -\log k_{\Delta t}(x\,|\,y) + \log\tilde{r}_{\Delta t}(y\,|\,x) + \log\frac{r_{\Delta t}(y\,|\,x)}{\tilde{r}_{\Delta t}(y\,|\,x)}\,, \tag{84}$$

where the last term involves the unknown reversed kernel. This term can typically be approximated by taking the divergence of the score (see Lemma 1), but due to the computational challenge of estimating the divergence we opt for a different strategy. Instead, in the following theorem, we study the distribution of the last term for different samples y generated from x and argue that this term can be ignored.

Theorem 3. [Detailed balance density estimator error] *For $y = x + \Delta t\cdot v + g_{t+\Delta t}\sqrt{\Delta t}\varepsilon$, where $g_{t+\Delta t} = \sqrt{2\sigma_t^2\frac{\partial}{\partial t}\log\frac{\sigma_t}{\alpha_t}}$ and ε is a standard normal random variable, the following estimator is unbiased w.r.t. the generated samples y, i.e.*

$$\mathbb{E}_\varepsilon\left[\log\frac{r_{\Delta t}(y\,|\,x)}{\tilde{r}_{\Delta t}(y\,|\,x)}\right] = o(\Delta t)\,, \tag{85}$$

and the variance is

$$\mathbf{D}_\varepsilon\left[\log\frac{r_{\Delta t}(y\,|\,x)}{\tilde{r}_{\Delta t}(y\,|\,x)}\right] = \Delta t^2\frac{g_{t+\Delta t}^4}{4}\mathbf{D}_\varepsilon\left(\varepsilon^T\frac{\partial^2\log q_t(x)}{\partial x^2}\varepsilon\right) + o(\Delta t^2)\,, \tag{86}$$

where $\frac{\partial^2\log q_{t+\Delta t}(x)}{\partial x^2}$ is the Hessian matrix of the log-density.

We postpone the proof of this theorem until App. D.4. Note that the last term in Eq. (84) has zero expectation and the same variance as Hutchinson's trace estimator. Thus, we argue that the following estimator is as efficient as the conventional divergence estimator with Hutchinson's trick

$$\log q_t(y) - \log q_{t+\Delta t}(x) \approx -\log k_{\Delta t}(x\,|\,y) + \log\tilde{r}_{\Delta t}(y\,|\,x)\,. \tag{87}$$

We further highlight that since the generation via the inference process happens in many steps with small Δt, we approximate the relation Eq. (87) up to the second order terms in Δt.

Proposition 11. [Recurrence relation for the log-density] *For $y = x + \Delta t\cdot v + g_{t+\Delta t}\sqrt{\Delta t}\varepsilon$, where $g_{t+\Delta t} = \sqrt{2\sigma_t^2\frac{\partial}{\partial t}\log\frac{\sigma_t}{\alpha_t}}$ and ε is a standard normal random variable, the estimator from Eq. (87) can be expanded as follows*

$$\begin{aligned}-\log k_{\Delta t}(x\,|\,y) + \log\tilde{r}_{\Delta t}(y\,|\,x) = d\Delta t\frac{\partial}{\partial t}\log\alpha_{t+\Delta t} - \Delta t\frac{g_{t+\Delta t}^2}{2}\|\nabla\log q_{t+\Delta t}(x)\|^2 + \\ +\left\langle\Delta t\cdot v + g_{t+\Delta t}\sqrt{\Delta t}\varepsilon + \Delta t\frac{\partial}{\partial t}\log\alpha_{t+\Delta t}x, \nabla\log q_{t+\Delta t}(x)\right\rangle + o(\Delta t)\end{aligned} \tag{88}$$

The proof for this proposition is included in App. D.5. For practical use cases we note that Eq. (88) is the final form of our density estimator.

D.1 Proof of Prop. 10

Proposition 10. [Universal noising kernel] *For any data density $p_{\mathrm{data}}(\mu)$, for the continuous noising process $q_t(x) = \int d\mu\,\mathcal{N}(x\,|\,\alpha_t\mu, \sigma_t^2)p_{\mathrm{data}}(\mu)$, there exists unique noising kernel*

$$k_{\Delta t}(x\,|\,y) = \mathcal{N}\left(x\,\middle|\,\frac{\alpha_{t+\Delta t}}{\alpha_t}y, S_{t+\Delta t}^2\right), q_{t+\Delta t}(x) = \int dy\; k_{\Delta t}(y\,|\,x)q_t(y), \tag{80}$$

where $S^2_{t+\Delta t} = \sigma^2_{t+\Delta t} - \sigma^2_t \frac{\alpha^2_{t+\Delta t}}{\alpha^2_t}$ *and it is independent of the densities* $p_{\text{data}}(\cdot), q_t(\cdot), q_{t+\Delta t}(\cdot)$.

Proof.

$$q_t(x) = \int d\mu \, \mathcal{N}(x \,|\, \alpha_t \mu, \sigma_t^2) p_{\text{data}}(\mu) \tag{89}$$

Let's derive the incremental kernel $k_{\Delta t}(x \,|\, y)$ from this formula, i.e.

$$q_{t+\Delta t}(x) = \int dy \; k_{\Delta t}(x \,|\, y) q_t(y) \tag{90}$$

$$\int d\mu \, \mathcal{N}(x \,|\, \alpha_{t+\Delta t}\mu, \sigma^2_{t+\Delta t}) p_{\text{data}}(\mu) = \int dy \; k_{\Delta t}(x \,|\, y) \int d\mu \, \mathcal{N}(y \,|\, \alpha_t \mu, \sigma_t^2) p_{\text{data}}(\mu) \tag{91}$$

$$\int d\mu \left(\mathcal{N}(x \,|\, \alpha_{t+\Delta t}\mu, \sigma^2_{t+\Delta t}) - \int dy \; k_{\Delta t}(x \,|\, y) \mathcal{N}(y \,|\, \alpha_t \mu, \sigma_t^2) \right) p_{\text{data}}(\mu) = 0 \tag{92}$$

$$\mathcal{N}(x \,|\, \alpha_{t+\Delta t}\mu, \sigma^2_{t+\Delta t}) = \int dy \; k_{\Delta t}(x \,|\, y) \mathcal{N}(y \,|\, \alpha_t \mu, \sigma_t^2) \tag{93}$$

$$x = \alpha_{t+\Delta t}\mu + \frac{y - \alpha_t \mu}{\sigma_t} S + R\varepsilon \,, \text{ where } \; y \sim \mathcal{N}(y \,|\, \alpha_t \mu, \sigma_t^2) \,, \text{ and } \varepsilon \sim \mathcal{N}(\varepsilon \,|\, 0, 1) \tag{94}$$

$$S^2 + R^2 = \sigma^2_{t+\Delta t} \tag{95}$$

To make the kernel independent of μ we have to choose $R = \sigma_t \frac{\alpha_{t+\Delta t}}{\alpha_t}$, then the kernel is

$$k_{\Delta t}(x \,|\, y) = \mathcal{N}\left(x \,|\, \frac{\alpha_{t+\Delta t}}{\alpha_t} y, \underbrace{\sigma^2_{t+\Delta t} - \sigma_t^2 \frac{\alpha^2_{t+\Delta t}}{\alpha_t^2}}_{S^2_{t+\Delta t}} \right) . \tag{96}$$

□

D.2 LEMMA 1

Lemma 1. [Reverse kernel lemma] *For the universal noising kernel* $k_{\Delta t}(x \,|\, y)$*, the corresponding reverse kernel* $r_{\Delta t}(y \,|\, x) = k_{\Delta t}(x \,|\, y) q_t(y) / q_{t+\Delta t}(x)$*, and its Gaussian approximation*

$$\tilde{r}_{\Delta t}(y \,|\, x) = \mathcal{N}\left(y \,\middle|\, \frac{\alpha_t}{\alpha_{t+\Delta t}} x + \frac{\alpha_t}{\alpha_{t+\Delta t}} S^2_{t+\Delta t} \nabla \log q_{t+\Delta t}(x), \left(\frac{\alpha_t}{\alpha_{t+\Delta t}} S_{t+\Delta t} \right)^2 \right) , \tag{97}$$

we have

$$\log \frac{r_{\Delta t}(x + \Delta t \cdot v + g_{t+\Delta t}\sqrt{\Delta t}\varepsilon \,|\, x)}{\tilde{r}_{\Delta t}(x + \Delta t \cdot v + g_{t+\Delta t}\sqrt{\Delta t}\varepsilon \,|\, x)} = \tag{98}$$

$$= \Delta t \cdot \frac{g^2_{t+\Delta t}}{2} \left(\Delta \log q_{t+\Delta t}(x) - \varepsilon^T \frac{\partial^2 \log q_t(x)}{\partial x^2} \varepsilon \right) + o(\Delta t) \,, \tag{99}$$

where $g_{t+\Delta t} = \sqrt{2\sigma^2_{t+\Delta t} \frac{\partial}{\partial t} \log \frac{\sigma_{t+\Delta t}}{\alpha_{t+\Delta t}}}$.

Proof. From the detailed balance equation, we have

$$\log r_{\Delta t}(y \,|\, x) = \log k_{\Delta t}(x \,|\, y) + \log q_t(y) - \log q_{t+\Delta t}(x) \tag{100}$$

$$= \frac{-1}{2S^2_{t+\Delta t}} \left(x - \frac{\alpha_{t+\Delta t}}{\alpha_t} y \right)^2 - \frac{d}{2} \log 2\pi S^2_{t+\Delta t} + \log q_t(y) - \log q_{t+\Delta t}(x) \,, \tag{101}$$

where we use the definition of the forward kernel. Thus, the difference between kernels is

$$\log \frac{r_{\Delta t}(y \,|\, x)}{\tilde{r}_{\Delta t}(y \,|\, x)} = \frac{-1}{2S_{t+\Delta t}^2}\left(x - \frac{\alpha_{t+\Delta t}}{\alpha_t} y\right)^2 - \frac{d}{2}\log 2\pi S_{t+\Delta t}^2 + \log q_t(y) - \log q_{t+\Delta t}(x) + \tag{102}$$

$$+ \frac{1}{2(S_{t+\Delta t}\frac{\alpha_t}{\alpha_{t+\Delta t}})^2}\left(y - \frac{\alpha_t}{\alpha_{t+\Delta t}} x - \frac{\alpha_t}{\alpha_{t+\Delta t}} S_{t+\Delta t}^2 \nabla \log q_{t+\Delta t}(x)\right)^2 + \tag{103}$$

$$+ \frac{d}{2}\log 2\pi S_{t+\Delta t}^2 + \frac{d}{2}\log\left(\frac{\alpha_t}{\alpha_{t+\Delta t}}\right)^2 . \tag{104}$$

Opening the brackets, we have

$$\log \frac{r_{\Delta t}(y \,|\, x)}{\tilde{r}_{\Delta t}(y \,|\, x)} = \cancel{\frac{-1}{2S_{t+\Delta t}^2}\left(x - \frac{\alpha_{t+\Delta t}}{\alpha_t} y\right)^2} + \log q_t(y) - \log q_{t+\Delta t}(x) + \tag{105}$$

$$+ \cancel{\frac{1}{2S_{t+\Delta t}^2}\left(\frac{\alpha_{t+\Delta t}}{\alpha_t} y - x\right)^2} - \left\langle \frac{\alpha_{t+\Delta t}}{\alpha_t} y - x, \nabla \log q_{t+\Delta t}(x)\right\rangle + \tag{106}$$

$$+ \frac{S_{t+\Delta t}^2}{2}\|\nabla \log q_{t+\Delta t}(x)\|^2 + \frac{d}{2}\log\left(\frac{\alpha_t}{\alpha_{t+\Delta t}}\right)^2 . \tag{107}$$

The constants can be estimated as follows

$$S_{t+\Delta t}^2 = \sigma_{t+\Delta t}^2 - \sigma_t^2 \frac{\alpha_{t+\Delta t}^2}{\alpha_t^2} = \sigma_{t+\Delta t}^2 - (\sigma_{t+\Delta t}^2 - 2dt\sigma_{t+\Delta t}\frac{\partial \sigma_{t+\Delta t}}{\partial t} + o(\Delta t))\frac{\alpha_{t+\Delta t}^2}{\alpha_t^2} \tag{108}$$

$$= \sigma_{t+\Delta t}^2 - (\sigma_{t+\Delta t}^2 - 2dt\sigma_{t+\Delta t}\frac{\partial \sigma_{t+\Delta t}}{\partial t} + o(\Delta t))\left(1 + 2dt\frac{\alpha_{t+\Delta t}^2}{\alpha_{t+\Delta t}^3}\frac{\partial \alpha_{t+\Delta t}}{\partial t} + o(\Delta t)\right) \tag{109}$$

$$= 2dt\sigma_{t+\Delta t}^2 \frac{\partial}{\partial t}\log\frac{\sigma_{t+\Delta t}}{\alpha_{t+\Delta t}} + o(\Delta t)\,, \tag{110}$$

and

$$\frac{\alpha_{t+\Delta t}}{\alpha_t} = 1 - \frac{\alpha_{t+\Delta t}}{\alpha_{t+\Delta t}^2}\frac{\partial \alpha_{t+\Delta t}}{\partial t}(-\Delta t) + o(\Delta t) = 1 + \Delta t \frac{\partial \log \alpha_{t+\Delta t}}{\partial t} + o(\Delta t) \tag{111}$$

$$\frac{d}{2}\log\left(\frac{\alpha_t}{\alpha_{t+\Delta t}}\right)^2 = -dtd\frac{\partial}{\partial t}\log \alpha_{t+\Delta t} + o(\Delta t)\,. \tag{112}$$

Thus, we have

$$\log \frac{r_{\Delta t}(y \,|\, x)}{\tilde{r}_{\Delta t}(y \,|\, x)} = \log q_t(y) - \log q_{t+\Delta t}(x) + \Delta t \sigma_{t+\Delta t}^2 \frac{\partial}{\partial t}\log\frac{\sigma_{t+\Delta t}}{\alpha_{t+\Delta t}}\|\nabla \log q_{t+\Delta t}(x)\|^2 - \tag{113}$$

$$-dtd\frac{\partial}{\partial t}\log \alpha_{t+\Delta t} - \left\langle (1 + \Delta t \frac{\partial \log \alpha_{t+\Delta t}}{\partial t})y - x, \nabla \log q_{t+\Delta t}(x)\right\rangle + o(\Delta t)\,. \tag{114}$$

From Prop. 8, the time-derivative of the density is

$$\frac{\partial}{\partial t}\log q_t(x) = -\left\langle \nabla, v_t(x)\right\rangle - \left\langle \nabla \log q_t(x), v_t(x)\right\rangle \tag{115}$$

$$= -d\frac{\partial \log \alpha_t}{\partial t} + \left(\sigma_t^2 \frac{\partial}{\partial t}\log\frac{\sigma_t}{\alpha_t}\right)\Delta \log q_t(x) - \tag{116}$$

$$- \frac{\partial \log \alpha_t}{\partial t}\left\langle \nabla \log q_t(x), x\right\rangle + \left(\sigma_t^2 \frac{\partial}{\partial t}\log\frac{\sigma_t}{\alpha_t}\right)\|\nabla \log q_t(x)\|^2 . \tag{117}$$

Hence, we have

$$\log q_t(x) - \log q_{t+\Delta t}(x) = -\Delta t \frac{\partial}{\partial t} \log q_{t+\Delta t}(x) + o(\Delta t) \tag{118}$$

$$= dtd \frac{\partial \log \alpha_{t+\Delta t}}{\partial t} - \Delta t \left(\sigma_{t+\Delta t}^2 \frac{\partial}{\partial t} \log \frac{\sigma_{t+\Delta t}}{\alpha_{t+\Delta t}} \right) \Delta \log q_{t+\Delta t}(x) + \tag{119}$$

$$+ \Delta t \frac{\partial \log \alpha_{t+\Delta t}}{\partial t} \left\langle \nabla \log q_{t+\Delta t}(x), x \right\rangle - \Delta t \left(\sigma_{t+\Delta t}^2 \frac{\partial}{\partial t} \log \frac{\sigma_{t+\Delta t}}{\alpha_{t+\Delta t}} \right) \| \nabla \log q_{t+\Delta t}(x) \|^2 . \tag{120}$$

Using it in Eq. (114), we have

$$\log \frac{r_{\Delta t}(y \,|\, x)}{\tilde{r}_{\Delta t}(y \,|\, x)} = \log q_t(y) - \log q_t(x) - \Delta t \left(\sigma_{t+\Delta t}^2 \frac{\partial}{\partial t} \log \frac{\sigma_{t+\Delta t}}{\alpha_{t+\Delta t}} \right) \Delta \log q_{t+\Delta t}(x) - \tag{121}$$

$$-(1 + \Delta t \frac{\partial \log \alpha_{t+\Delta t}}{\partial t}) \langle y - x, \nabla \log q_{t+\Delta t}(x) \rangle + o(\Delta t) . \tag{122}$$

Finally, we consider $y = x + \Delta t \cdot v + g_{t+\Delta t} \sqrt{\Delta t} \varepsilon$. Then we can estimate

$$\log q_t(y) = \log q_t(x) + \left\langle \nabla \log q_t(x), y - x \right\rangle + \frac{1}{2} (y - x)^T \frac{\partial^2 \log q_t(x)}{\partial x^2} (y - x) \tag{123}$$

$$+ o(\|y - x\|^2) \tag{124}$$

$$= \log q_t(x) + \left\langle \nabla \log q_t(x), \Delta t \cdot v + g_{t+\Delta t} \sqrt{\Delta t} \varepsilon \right\rangle \tag{125}$$

$$+ \Delta t \frac{g_{t+\Delta t}^2}{2} \varepsilon^T \frac{\partial^2 \log q_t(x)}{\partial x^2} \varepsilon + o(\Delta t) , \tag{126}$$

where $\frac{\partial^2 \log q_t(x)}{\partial x^2}$ denotes the Hessian of the log-density. Thus, for $y = x + \Delta t \cdot v + g_{t+\Delta t} \sqrt{\Delta t} \varepsilon$, we have

$$\log \frac{r_{\Delta t}(y \,|\, x)}{\tilde{r}_{\Delta t}(y \,|\, x)} = \Delta t \frac{g_{t+\Delta t}^2}{2} \varepsilon^T \frac{\partial^2 \log q_t(x)}{\partial x^2} \varepsilon - \Delta t \left(\sigma_{t+\Delta t}^2 \frac{\partial}{\partial t} \log \frac{\sigma_{t+\Delta t}}{\alpha_{t+\Delta t}} \right) \Delta \log q_{t+\Delta t}(x) + \tag{127}$$

$$+ \left\langle \nabla \log q_t(x) - \nabla \log q_{t+\Delta t}(x), \Delta t \cdot v + g_{t+\Delta t} \sqrt{\Delta t} \varepsilon \right\rangle + o(\Delta t) . \tag{128}$$

The last term is $o(\Delta t)$ by expanding the scores in time, hence, for $\frac{g_{t+\Delta t}^2}{2} = \sigma_{t+\Delta t}^2 \frac{\partial}{\partial t} \log \frac{\sigma_{t+\Delta t}}{\alpha_{t+\Delta t}}$, we have

$$\log \frac{r_{\Delta t}(x + \Delta t \cdot v + g_{t+\Delta t} \sqrt{\Delta t} \varepsilon \,|\, x)}{\tilde{r}_{\Delta t}(x + \Delta t \cdot v + g_{t+\Delta t} \sqrt{\Delta t} \varepsilon \,|\, x)} = \tag{129}$$

$$= \Delta t \left(\sigma_{t+\Delta t}^2 \frac{\partial}{\partial t} \log \frac{\sigma_{t+\Delta t}}{\alpha_{t+\Delta t}} \right) \left(\Delta \log q_{t+\Delta t}(x) - \varepsilon^T \frac{\partial^2 \log q_t(x)}{\partial x^2} \varepsilon \right) + o(\Delta t) . \tag{130}$$

□

D.3 Proof of Thm. 2

Theorem 2. [Denoising kernel] *For the universal noising kernel $k_{\Delta t}(x \,|\, y)$, the Gaussian approximation of the corresponding reverse kernel $r_{\Delta t}(y \,|\, x) = k_{\Delta t}(x \,|\, y) q_t(y) / q_{t+\Delta t}(x)$ is*

$$\tilde{r}_{\Delta t}(y \,|\, x) = \mathcal{N}\left(y \,\middle|\, \frac{\alpha_t}{\alpha_{t+\Delta t}} x + \frac{\alpha_t}{\alpha_{t+\Delta t}} S_{t+\Delta t}^2 \nabla \log q_{t+\Delta t}(x), \left(\frac{\alpha_t}{\alpha_{t+\Delta t}} S_{t+\Delta t} \right)^2 \right) , \tag{81}$$

which corresponds to a single step of the Euler discretization of the following SDE

$$dx_\tau = -\left(\frac{\partial}{\partial t} \log \alpha_t x - 2\sigma_t^2 \frac{\partial}{\partial t} \log \frac{\sigma_t}{\alpha_t} \nabla_x \log q_t(x) \right) \cdot d\tau + \sqrt{2\sigma_t^2 \frac{\partial}{\partial t} \log \frac{\sigma_t}{\alpha_t}} dW_\tau , \tag{82}$$

and

$$D_{\mathrm{KL}}(\tilde{r}_{\Delta t}(y \,|\, x) \| r_{\Delta t}(y \,|\, x)) = o(\Delta t) . \tag{83}$$

Proof. To find the reverse the kernel, we first use Tweedie's formula to find the expectation, i.e.

$$\nabla \log q_{t+\Delta t}(x) = -\frac{1}{q_{t+\Delta t}(x)} \int dy \, \frac{1}{S_{t+\Delta t}^2} \left(x - \frac{\alpha_{t+\Delta t}}{\alpha_t} y \right) k_{\Delta t}(x \,|\, y) q_t(y) \tag{131}$$

$$\frac{\alpha_t}{\alpha_{t+\Delta t}} S_{t+\Delta t}^2 \nabla \log q_{t+\Delta t}(x) = -\frac{1}{q_{t+\Delta t}(x)} \int dy \, \left(\frac{\alpha_t}{\alpha_{t+\Delta t}} x - y \right) k_{\Delta t}(x \,|\, y) q_t(y) \tag{132}$$

$$\frac{\alpha_t}{\alpha_{t+\Delta t}} x + \frac{\alpha_t}{\alpha_{t+\Delta t}} S_{t+\Delta t}^2 \nabla \log q_{t+\Delta t}(x) = \int dy \, y \frac{k_{\Delta t}(x \,|\, y) q_t(y)}{q_{t+\Delta t}(x)} = \int dy \, y r_{\Delta t}(y \,|\, x) \,. \tag{133}$$

Thus, we are going to approximate

$$\tilde{r}_{\Delta t}(y \,|\, x) = \mathcal{N}\left(y \,\middle|\, \frac{\alpha_t}{\alpha_{t+\Delta t}} x + \frac{\alpha_t}{\alpha_{t+\Delta t}} S_{t+\Delta t}^2 \nabla \log q_{t+\Delta t}(x), \left(\frac{\alpha_t}{\alpha_{t+\Delta t}} S_{t+\Delta t} \right)^2 \right) \tag{134}$$

where $\left(\frac{\alpha_t}{\alpha_{t+\Delta t}} S_{t+\Delta t} \right)^2$ is chosen to match the leading term of $k_{\Delta t}(x \,|\, y)$. The constants can be estimated as follows

$$S_{t+\Delta t}^2 = \sigma_{t+\Delta t}^2 - \sigma_t^2 \frac{\alpha_{t+\Delta t}^2}{\alpha_t^2} = \sigma_{t+\Delta t}^2 - (\sigma_{t+\Delta t}^2 - 2dt \sigma_{t+\Delta t} \frac{\partial \sigma_{t+\Delta t}}{\partial t} + o(\Delta t)) \frac{\alpha_{t+\Delta t}^2}{\alpha_t^2} \tag{135}$$

$$= \sigma_{t+\Delta t}^2 - (\sigma_{t+\Delta t}^2 - 2dt \sigma_{t+\Delta t} \frac{\partial \sigma_{t+\Delta t}}{\partial t} + o(\Delta t)) \left(1 + 2dt \frac{\alpha_{t+\Delta t}^2}{\alpha_{t+\Delta t}^3} \frac{\partial \alpha_{t+\Delta t}}{\partial t} + o(\Delta t) \right) \tag{136}$$

$$= 2dt \sigma_{t+\Delta t}^2 \frac{\partial}{\partial t} \log \frac{\sigma_{t+\Delta t}}{\alpha_{t+\Delta t}} + o(\Delta t) \,, \tag{137}$$

and

$$\frac{\alpha_t}{\alpha_{t+\Delta t}} = 1 + \frac{1}{\alpha_{t+\Delta t}} \frac{\partial \alpha_{t+\Delta t}}{\partial t} (-\Delta t) + o(\Delta t) = 1 - \Delta t \frac{\partial \log \alpha_{t+\Delta t}}{\partial t} + o(\Delta t) \,. \tag{138}$$

Thus, y can be generated as

$$y = x - \Delta t \frac{\partial \log \alpha_{t+\Delta t}}{\partial t} x + 2dt \sigma_{t+\Delta t}^2 \frac{\partial}{\partial t} \log \frac{\sigma_{t+\Delta t}}{\alpha_{t+\Delta t}} \nabla \log q_{t+\Delta t}(x) + \tag{139}$$

$$+ \sqrt{2dt \sigma_{t+\Delta t}^2 \frac{\partial}{\partial t} \log \frac{\sigma_{t+\Delta t}}{\alpha_{t+\Delta t}}} \varepsilon \,, \tag{140}$$

where ε is a standard normal random variable. This corresponds to the single step of the Euler discretization of the following SDE

$$dx_t = -\left(\frac{\partial}{\partial t} \log \alpha_t x - 2\sigma_t^2 \frac{\partial}{\partial t} \log \frac{\sigma_t}{\alpha_t} \nabla_x \log q_t(x) \right) \cdot \Delta t + \sqrt{2\sigma_t^2 \frac{\partial}{\partial t} \log \frac{\sigma_t}{\alpha_t}} dW_t \,. \tag{141}$$

For the KL-divergence between the reverse kernel and its Gaussian approximation, we have

$$D_{\mathrm{KL}}(\tilde{r}_{\Delta t}(y \,|\, x) \| r_{\Delta t}(y \,|\, x)) = \mathbb{E}_\varepsilon \log \frac{\tilde{r}_{\Delta t}(x + \Delta t \cdot v + g_{t+\Delta t} \sqrt{\Delta t} \varepsilon \,|\, x)}{r_{\Delta t}(x + \Delta t \cdot v + g_{t+\Delta t} \sqrt{\Delta t} \varepsilon \,|\, x)} + o(\Delta t) \,, \tag{142}$$

where

$$v = -\left(\frac{\partial}{\partial t} \log \alpha_t x - 2\sigma_t^2 \frac{\partial}{\partial t} \log \frac{\sigma_t}{\alpha_t} \nabla_x \log q_t(x) \right), \quad \text{and} \quad g_{t+\Delta t} = \sqrt{2\sigma_t^2 \frac{\partial}{\partial t} \log \frac{\sigma_t}{\alpha_t}} \,. \tag{143}$$

From Lemma 1, we have

$$D_{\mathrm{KL}} \left(\tilde{r}_{\Delta t}(y \,|\, x) \| r_{\Delta t}(y \,|\, x) \right) = \tag{144}$$

$$= \Delta t \left(\sigma_{t+\Delta t}^2 \frac{\partial}{\partial t} \log \frac{\sigma_{t+\Delta t}}{\alpha_{t+\Delta t}} \right) \mathbb{E}_\varepsilon \left(\varepsilon^T \frac{\partial^2 \log q_t(x)}{\partial x^2} \varepsilon - \Delta \log q_{t+\Delta t}(x) \right) + o(\Delta t) \tag{145}$$

$$= o(\Delta t) \,. \tag{146}$$

□

D.4 Proof of Thm. 3

Theorem 3. [Detailed balance density estimator error] *For $y = x + \Delta t \cdot v + g_{t+\Delta t}\sqrt{\Delta t}\varepsilon$, where $g_{t+\Delta t} = \sqrt{2\sigma_t^2 \frac{\partial}{\partial t} \log \frac{\sigma_t}{\alpha_t}}$ and ε is a standard normal random variable, the following estimator is unbiased w.r.t. the generated samples y, i.e.*

$$\mathbb{E}_\varepsilon \left[\log \frac{r_{\Delta t}(y \,|\, x)}{\tilde{r}_{\Delta t}(y \,|\, x)} \right] = o(\Delta t)\,, \tag{85}$$

and the variance is

$$\mathbf{D}_\varepsilon \left[\log \frac{r_{\Delta t}(y \,|\, x)}{\tilde{r}_{\Delta t}(y \,|\, x)} \right] = \Delta t^2 \frac{g_{t+\Delta t}^4}{4} \mathbf{D}_\varepsilon \left(\varepsilon^T \frac{\partial^2 \log q_t(x)}{\partial x^2} \varepsilon \right) + o(\Delta t^2)\,, \tag{86}$$

where $\frac{\partial^2 \log q_{t+\Delta t}(x)}{\partial x^2}$ is the Hessian matrix of the log-density.

Proof. From Lemma 1, we have

$$\mathbb{E}_\varepsilon \log \frac{r_{\Delta t}(y \,|\, x)}{\tilde{r}_{\Delta t}(y \,|\, x)} = \mathbb{E}_\varepsilon \Delta t \frac{g_{t+\Delta t}^2}{2} \left(\Delta \log q_{t+\Delta t}(x) - \varepsilon^T \frac{\partial^2 \log q_t(x)}{\partial x^2} \varepsilon \right) + o(\Delta t) \tag{147}$$

$$= \Delta t \frac{g_{t+\Delta t}^2}{2} \left(\Delta \log q_{t+\Delta t}(x) - \mathbb{E}_\varepsilon \operatorname{Tr} \left[\varepsilon^T \frac{\partial^2 \log q_t(x)}{\partial x^2} \varepsilon \right] \right) + o(\Delta t) \tag{148}$$

$$= \Delta t \frac{g_{t+\Delta t}^2}{2} \left(\Delta \log q_{t+\Delta t}(x) - \mathbb{E}_\varepsilon \operatorname{Tr} \left[\frac{\partial^2 \log q_t(x)}{\partial x^2} \right] \right) + o(\Delta t) \tag{149}$$

$$= o(\Delta t)\,. \tag{150}$$

For the variance, we have

$$\mathbf{D}_\varepsilon \log \frac{r_{\Delta t}(y \,|\, x)}{\tilde{r}_{\Delta t}(y \,|\, x)} = \Delta t^2 \frac{g_{t+\Delta t}^4}{4} \mathbb{E}_\varepsilon \left(\Delta \log q_{t+\Delta t}(x) - \varepsilon^T \frac{\partial^2 \log q_t(x)}{\partial x^2} \varepsilon \right)^2 + o(\Delta t^2) \tag{151}$$

$$= \Delta t^2 \frac{g_{t+\Delta t}^4}{4} \mathbb{E}_\varepsilon \left(\mathbb{E}_\eta \left[\eta^T \frac{\partial^2 \log q_t(x)}{\partial x^2} \eta \right] - \varepsilon^T \frac{\partial^2 \log q_t(x)}{\partial x^2} \varepsilon \right)^2 + o(\Delta t^2) \tag{152}$$

$$= \Delta t^2 \frac{g_{t+\Delta t}^4}{4} \mathbf{D}_\varepsilon \left(\varepsilon^T \frac{\partial^2 \log q_t(x)}{\partial x^2} \varepsilon \right) + o(\Delta t^2)\,, \tag{153}$$

where we used a standard normal random variable η. □

D.5 Proof of Prop. 11

Proposition 11. [Recurrence relation for the log-density] *For $y = x + \Delta t \cdot v + g_{t+\Delta t}\sqrt{\Delta t}\varepsilon$, where $g_{t+\Delta t} = \sqrt{2\sigma_t^2 \frac{\partial}{\partial t} \log \frac{\sigma_t}{\alpha_t}}$ and ε is a standard normal random variable, the estimator from Eq. (87) can be expanded as follows*

$$-\log k_{\Delta t}(x \,|\, y) + \log \tilde{r}_{\Delta t}(y \,|\, x) = d\Delta t \frac{\partial}{\partial t} \log \alpha_{t+\Delta t} - \Delta t \frac{g_{t+\Delta t}^2}{2} \|\nabla \log q_{t+\Delta t}(x)\|^2 + \\ + \left\langle \Delta t \cdot v + g_{t+\Delta t}\sqrt{\Delta t}\varepsilon + \Delta t \frac{\partial}{\partial t} \log \alpha_{t+\Delta t} x, \nabla \log q_{t+\Delta t}(x) \right\rangle + o(\Delta t) \tag{88}$$

Proof. Indeed,

$$\log \frac{\tilde{r}_{\Delta t}(y \,|\, x)}{k_{\Delta t}(x \,|\, y)} = \frac{1}{2B_{t+\Delta t}^2}\left(x - \frac{\alpha_{t+\Delta t}}{\alpha_t}y\right)^2 + \frac{d}{2}\log 2\pi S_{t+\Delta t}^2 - \tag{154}$$

$$- \frac{1}{2(S_{t+\Delta t}\frac{\alpha_t}{\alpha_{t+\Delta t}})^2}\left(y - \frac{\alpha_t}{\alpha_{t+\Delta t}}x - \frac{\alpha_t}{\alpha_{t+\Delta t}}S_{t+\Delta t}^2 \nabla \log q_{t+\Delta t}(x)\right)^2 - \tag{155}$$

$$- \frac{d}{2}\log 2\pi S_{t+\Delta t}^2 - d\log\frac{\alpha_t}{\alpha_{t+\Delta t}} \tag{156}$$

$$= -d\log\frac{\alpha_t}{\alpha_{t+\Delta t}} + \left\langle \frac{\alpha_{t+\Delta t}}{\alpha_t}y - x, \nabla \log q_{t+\Delta t}(x)\right\rangle - \tag{157}$$

$$- \frac{S_{t+\Delta t}^2}{2}\|\nabla \log q_{t+\Delta t}(x)\|^2 \tag{158}$$

Expanding the time around $t + \Delta t$, we have

$$\log \frac{\tilde{r}_{\Delta t}(y \,|\, x)}{k_{\Delta t}(x \,|\, y)} = d\Delta t\frac{\partial}{\partial t}\log \alpha_{t+\Delta t} + \left\langle (1 + \Delta t\frac{\partial}{\partial t}\log \alpha_{t+\Delta t})y - x, \nabla \log q_{t+\Delta t}(x)\right\rangle - \tag{159}$$

$$- \Delta t\left(\sigma_{t+\Delta t}^2 \frac{\partial}{\partial t}\log\frac{\sigma_{t+\Delta t}}{\alpha_{t+\Delta t}}\right)\|\nabla \log q_{t+\Delta t}(x)\|^2 + o(\Delta t)\,. \tag{160}$$

For $y = x + \Delta t \cdot v + \sqrt{\Delta t}g_{t+\Delta t}\varepsilon,\ g_{t+\Delta t} = \sqrt{2\sigma_{t+\Delta t}^2 \frac{\partial}{\partial t}\log\frac{\sigma_{t+\Delta t}}{\alpha_{t+\Delta t}}}$, we have

$$\log \frac{\tilde{r}_{\Delta t}(y \,|\, x)}{k_{\Delta t}(x \,|\, y)} = d\Delta t\frac{\partial}{\partial t}\log \alpha_{t+\Delta t} - \Delta t\frac{g_{t+\Delta t}^2}{2}\|\nabla \log q_{t+\Delta t}(x)\|^2 + \tag{161}$$

$$+ \left\langle \Delta t \cdot v + g_{t+\Delta t}\sqrt{\Delta t}\varepsilon + \Delta t\frac{\partial}{\partial t}\log \alpha_{t+\Delta t}x, \nabla \log q_{t+\Delta t}(x)\right\rangle + o(\Delta t)\,. \tag{162}$$

□

E Broader Impacts

In this paper, we present theoretical results and demonstrate use cases in generation tasks such as image generation and unconditional protein generation. Because of the theoretical nature of our contributions, this work carries little societal impact. SuperDiff can be used to generated protein structure from a composition of existing protein diffusion models. Better protein generation methods can potentially lead to negative use in generating bio-hazardous molecules and proteins. We do not perceive this as a great risk at the current stage of these models.

F Additional results for CIFAR-10

Table A1: Image generation performance for CIFAR-10 with *conditional* models trained on two random partitions of the training data (labeled A and B). We compare SuperDiff (**OR**) with the respective models (model$_A$ and model$_B$) with the model that is trained on the full dataset (model$_{A\cup B}$) and random choice between two models (model$_{A \text{ OR } B}$).

	ODE inference			SDE inference		
	FID (↓)	IS (↑)	FLD (↓)	FID (↓)	IS (↑)	FLD (↓)
model$_A$	4.75	8.98	6.95 ± 0.12	4.66	9.35	6.39 ± 0.13
model$_B$	4.78	8.97	6.86 ± 0.15	4.36	**9.45**	$\mathbf{6.20 \pm 0.14}$
model$_{A\cup B}$	5.30	**9.04**	6.82 ± 0.09	**2.83**	9.44	6.26 ± 0.11
model$_{A \text{ OR } B}$	4.75	8.94	6.86 ± 0.15	4.41	9.40	6.3 ± 0.18
SuperDiff (**OR**)	4.74	9.00	6.98 ± 0.10	4.46	9.40	6.22 ± 0.15
SuperDiff $_{T=100}$ (**OR**)	**4.63**	8.98	$\mathbf{6.81 \pm 0.19}$	4.23	9.42	6.27 ± 0.12

G Protein generation

G.1 Experimental details

In our setting, we consider two state-of-the-art diffusion models for protein generation: Proteus (Wang et al., 2024) and FrameDiff (Yim et al., 2023b), which were trained on protein structures from Protein

Data Bank (PDB, (Berman et al., 2000)) to estimate the special Euclidean group (SE(3)) equivariant score over multiple diffusion steps. The models' outputs predict the coordinates of a monomeric protein backbone.

We use pre-trained checkpoints from Proteus[2] and FrameDiff[3]. During protein generation at inference, we separately combine scores for translations and rotations from both models using Algorithm 1.

We investigate the use of different temperature (T) settings to scale κ for controlling the densities. We also found that adding a small bias (ω) towards Proteus log densities improved designability.

G.2 Metrics for evaluating generated proteins

Designability. We assess designability using the *self-consistency* evaluation from Trippe et al. (2023), where given a generated backbone, we predict its scaffold using a sequence prediction model (we use ProteinMPNN (Dauparas et al., 2022)) and re-fold the sequence using a structure prediction model (we use ESMFold (Lin et al., 2022)). We then compare the re-folded protein to the original generated backbone by computing their template modeling score (`scTM`) and root-mean-square-distance (`scRMSD`). A protein is considered to be designable if its `scRMSD` is < 2Å to the refolded structure. For each protein, we repeat this process 8 times and keep the sequence with the lowest `scRMSD`. We report the fraction of designable proteins for each method in Table 3 as well as the `scRMSD` mean of the resulting *designable* proteins.

Novelty. A significant impetus for generative modelling in biology and chemistry is to propose compounds that have not been previously identified (i.e., different from the training data), but are also possible to make. We compute three novelty metrics: the fraction of designable proteins with a `scTM` score < 0.5 (higher is better), the fraction of designable proteins with a `scTM` score < 0.3, and the mean `scTM` score between generated proteins and the proteins from PDB that the original diffusion models were trained on, which represents the collective human knowledge of protein structures; a lower score is indicates higher distance from the training set and is desirable since it shows generalization ability.

Diversity. To measure how diverse the generated proteins are, we compute their mean pairwise `scTM` score (lower is better), and also report the fraction of unique clusters formed after clustering them with MaxCluster (Herbert & Sternberg, 2008) (higher is better). Finally, we report the fraction of proteins that contain β-sheet secondary structures, as it has been found that these structures are typically more rare to generate (Bose et al., 2024).

G.3 Protein diversity exploration settings

To embed and cluster the generated protein backbones we use the foldseek (Van Kempen et al., 2024) package to compute pairwise aligned TM-scores. We then use the UMAP (McInnes et al., 2018) package to compute a 2D embedding. Where proteins are represented as points that are close to each other if they are structurally similar (by aligned TM-Score).

We then clustered the proteins again with the foldseek tool to find representative structures. Finally we used KMeans to explore the space and narrow down which protein structures belong where on the protein structure manifold.

H Generating image compositions with Stable diffusion

For our concept interpolation experiments, we use publicly-available pre-trained weights, models, and schedulers from Stable Diffusion v1-4 `https://huggingface.co/CompVis/stable-diffusion-v1-4`.

In Figs. A1–A20, we show examples of image compositions generated by SuperDiff (**AND**), averaging of outputs, and joint prompting. Prompts are shown in each image caption. We show images generated by the first 6 seeds (uniform sampling), as well as our favourite images generated from 20 seeds. For joint prompting, we generate prompts from two concepts using the linking term `"that looks like"`. For example, given the concepts `"a lemon"` and `"a sunflower"`, the resulting prompt would be `"a sunflower that looks like a lemon"`. We also generate

[2] `https://github.com/Wangchentong/Proteus`
[3] `https://github.com/jasonkyuyim/se3_diffusion`

images with the reversed prompt (`"a lemon that looks like a sunflower"`), and keep the images generated by the prompt resulting in the higher mean score for each metric. The order of the concepts in each image caption reflects the ordering that obtained the higher TIFA score.

In Fig. A21, we show examples of image compositions generated by SuperDiff (**OR**), joint prompting, and an upper bound of randomly selecting a prompt of one concept. Again, we keep the prompt order that resulted in higher scores for the baseline.

Figure A1: Image compositions generated using SuperDiff (**AND**), averaging of outputs, or joint prompting for the concepts `"an airplane"` and `"an eagle"`.

Figure A2: Image compositions generated using SuperDiff (AND), averaging of outputs, or joint prompting for the concepts "bottle cap" and "chess pawn".

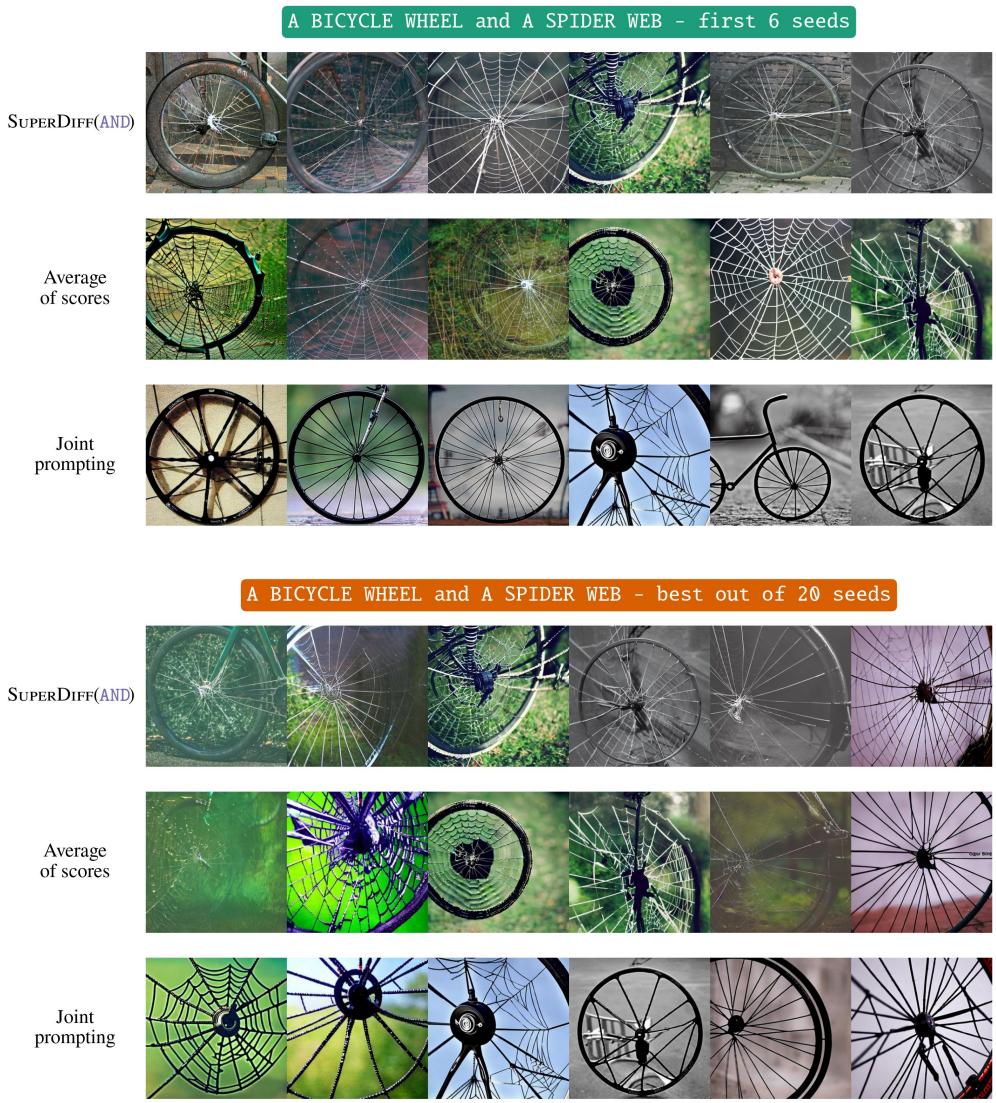

Figure A3: Image compositions generated using SuperDiff (**AND**), averaging of outputs, or joint prompting for the concepts "`a bicycle wheel`" and "`a spider web`".

Figure A4: Image compositions generated using SuperDiff (**AND**), averaging of outputs, or joint prompting for the concepts "`a chair`" and "`an avocado`".

Figure A5: Image compositions generated using SuperDiff (**AND**), averaging of outputs, or joint prompting for the concepts "`a cinnamon roll`" and "`a snail`".

Figure A6: Image compositions generated using SuperDiff (**AND**), averaging of outputs, or joint prompting for the concepts "`cookie`" and "`moon`".

Figure A7: Image compositions generated using SuperDiff (**AND**), averaging of outputs, or joint prompting for the concepts "`a dog`" and "`a cat`".

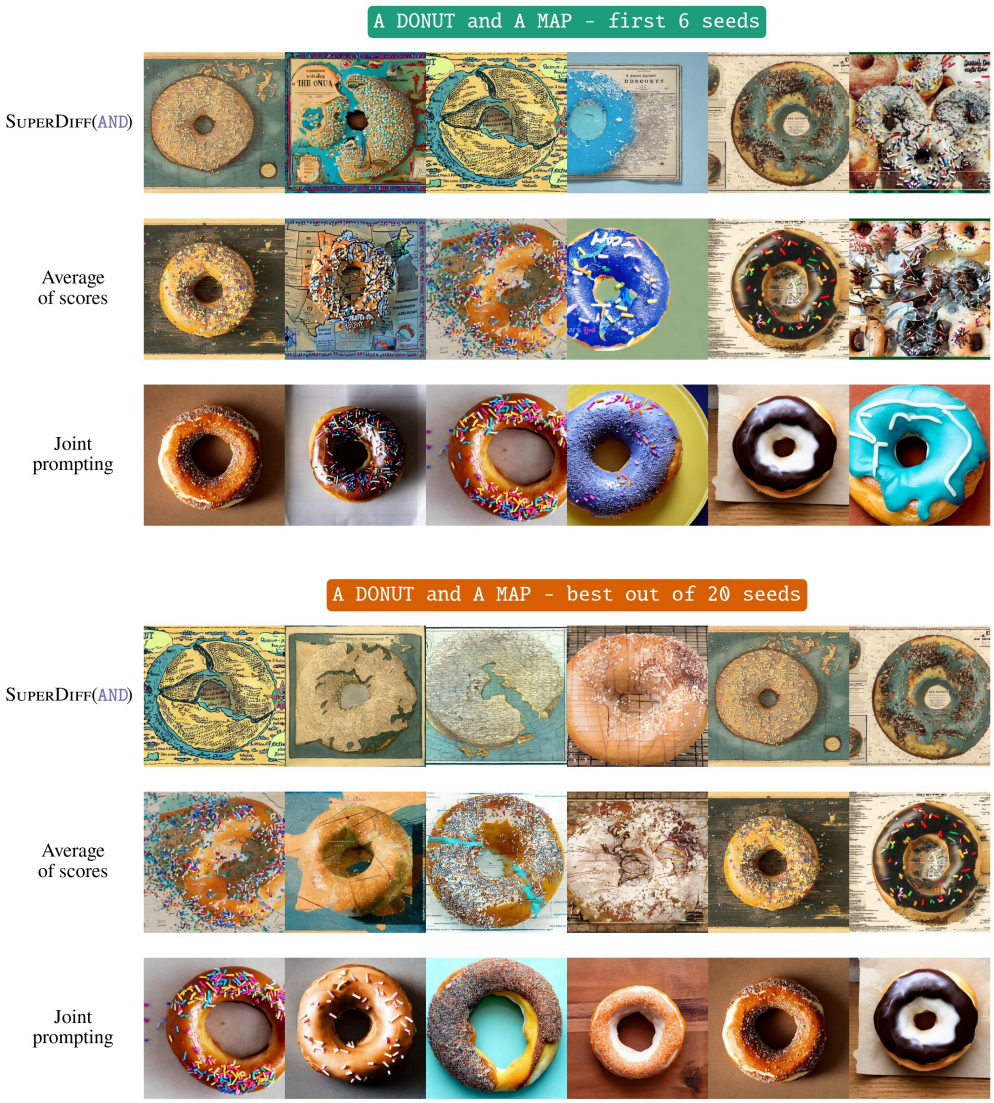

Figure A8: Image compositions generated using SuperDiff (**AND**), averaging of outputs, or joint prompting for the concepts "`a donut`" and "`a map`".

Figure A9: Image compositions generated using SuperDiff (**AND**), averaging of outputs, or joint prompting for the concepts "duck" and "otter".

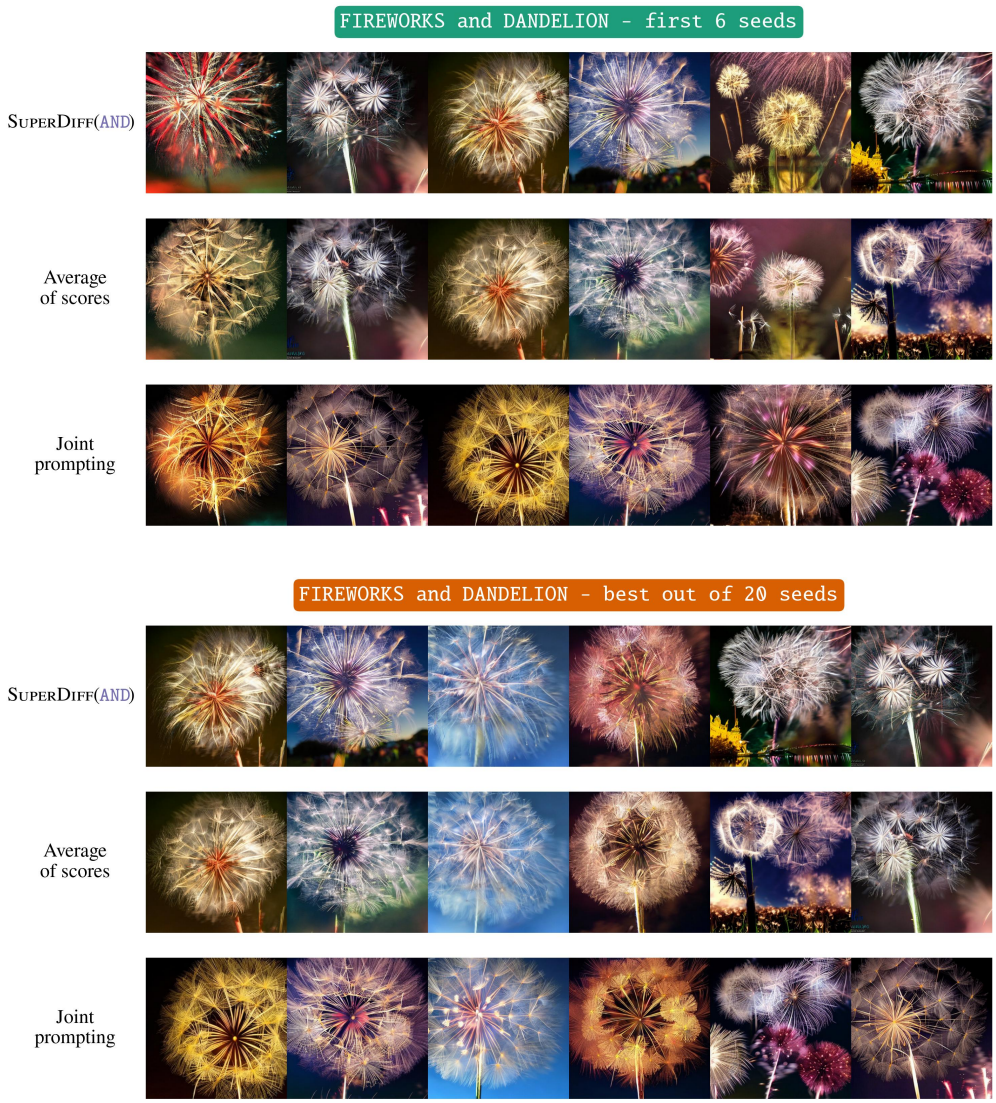

Figure A10: Image compositions generated using SuperDiff (**AND**), averaging of outputs, or joint prompting for the concepts "`fireworks`" and "`dandelion`".

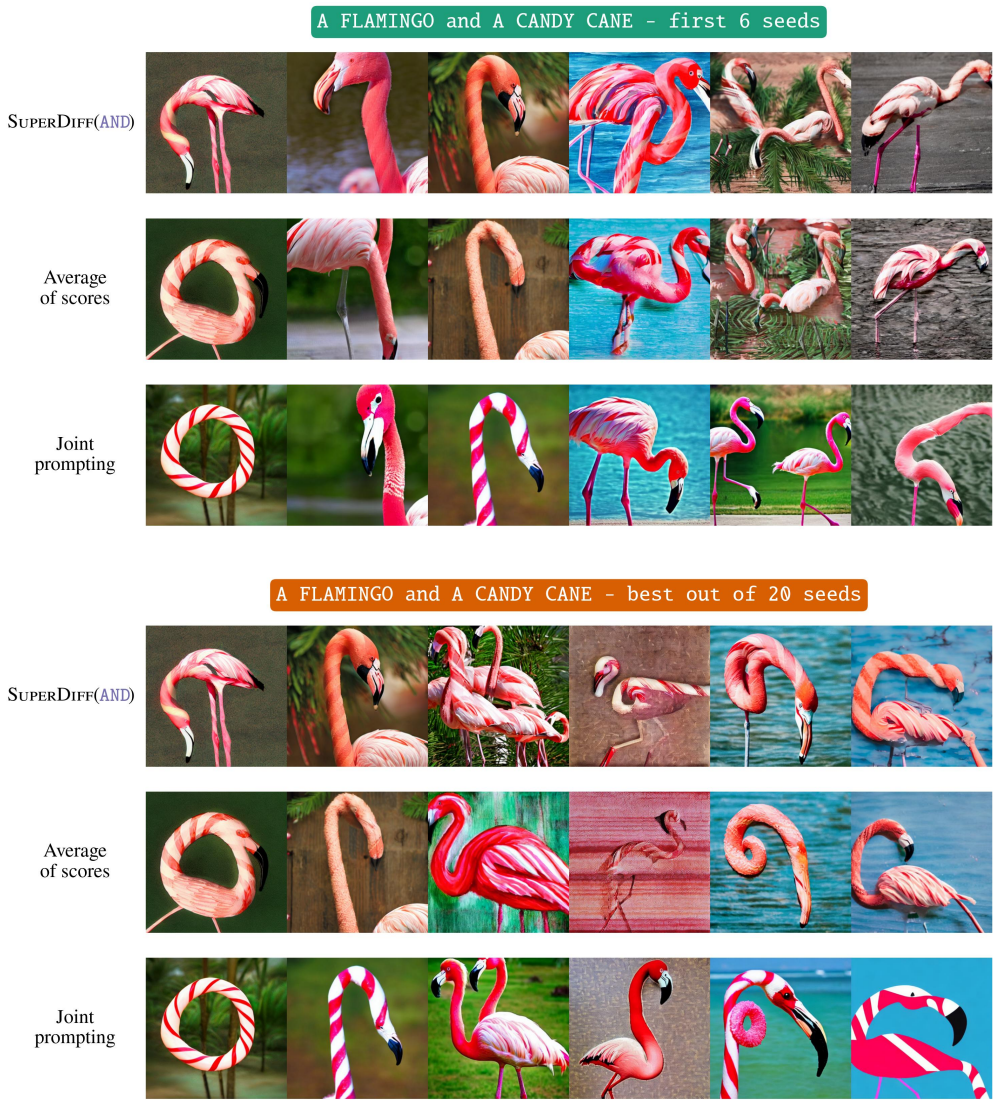

Figure A11: Image compositions generated using SuperDiff (**AND**), averaging of outputs, or joint prompting for the concepts "`a flamingo`" and "`a candy cane`".

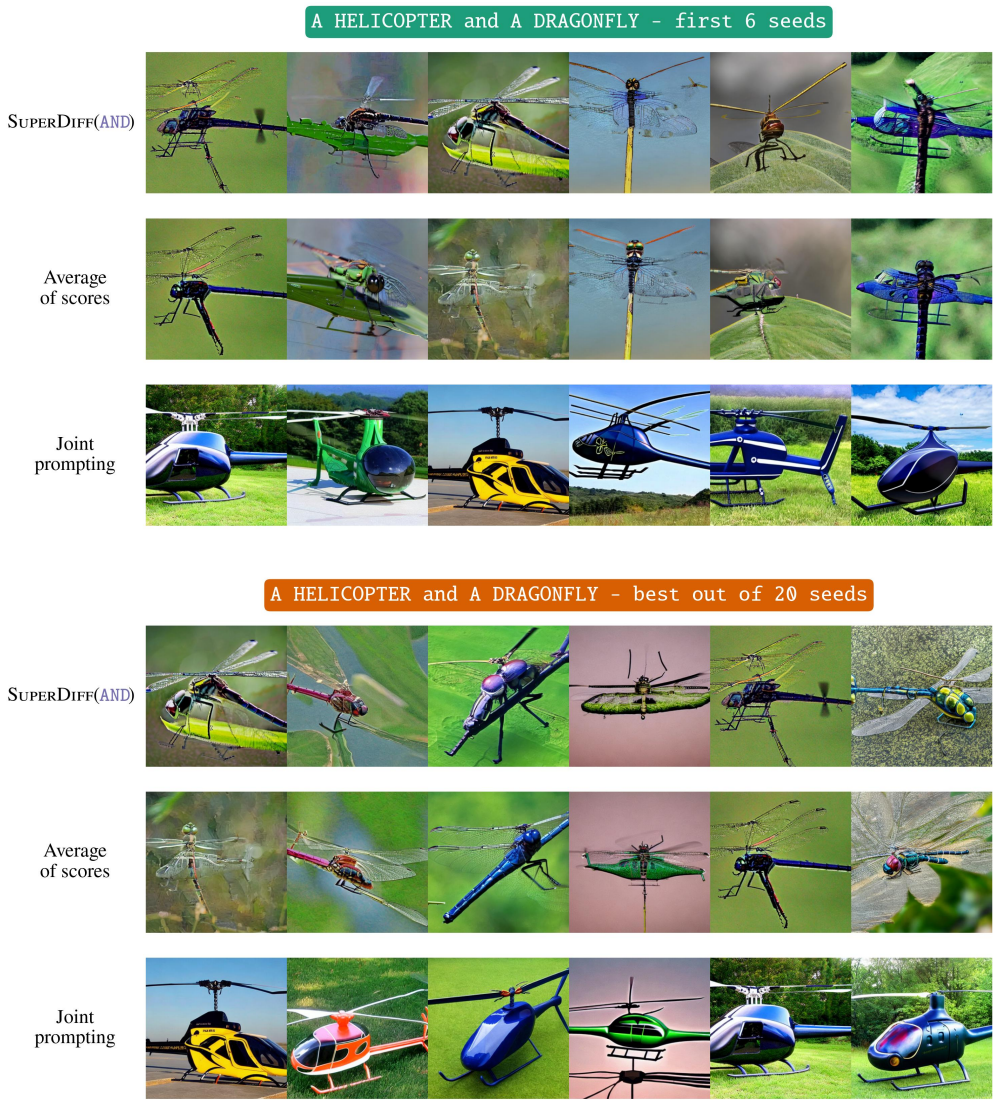

Figure A12: Image compositions generated using SuperDiff (**AND**), averaging of outputs, or joint prompting for the concepts "`a helicopter`" and "`a dragonfly`".

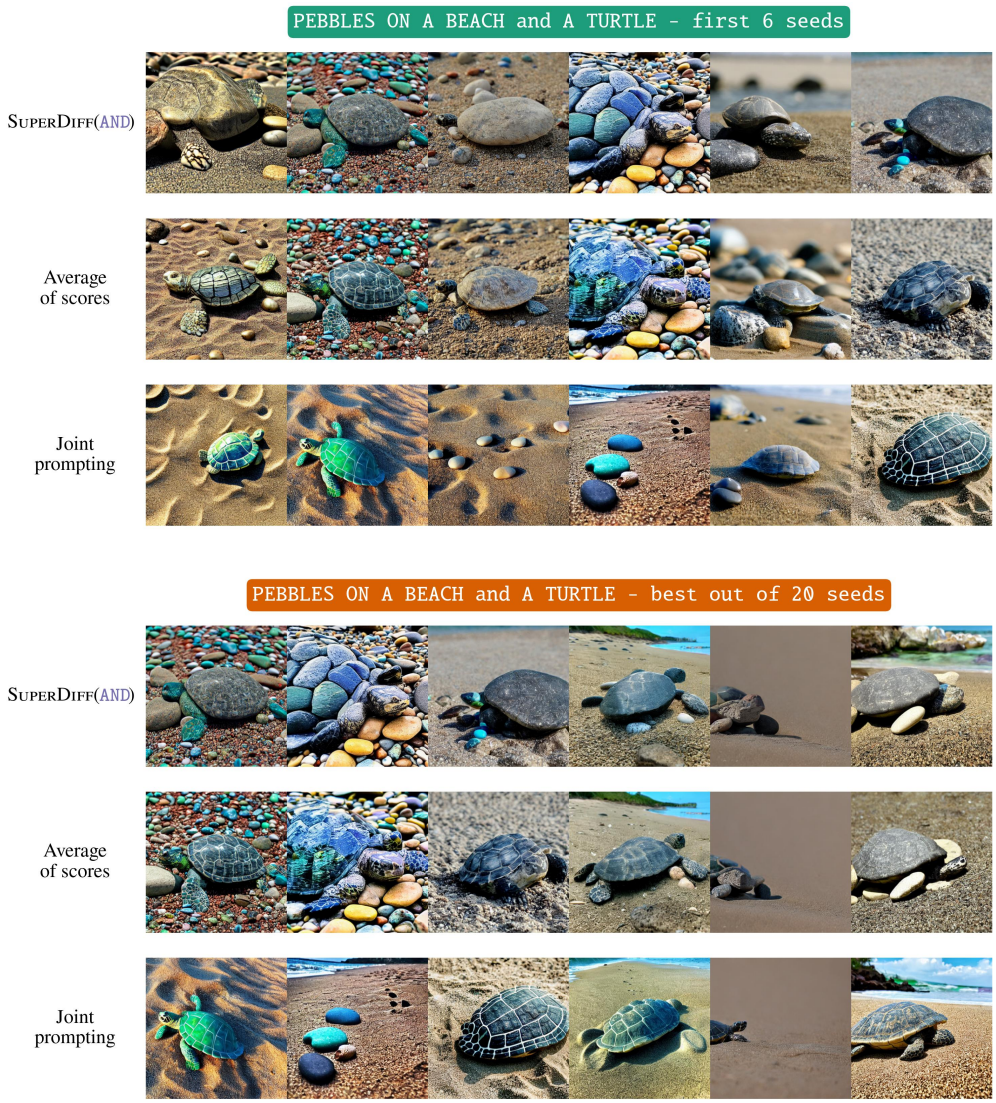

Figure A13: Image compositions generated using SuperDiff (**AND**), averaging of outputs, or joint prompting for the concepts "`pebbles on a beach`" and "`a turtle`".

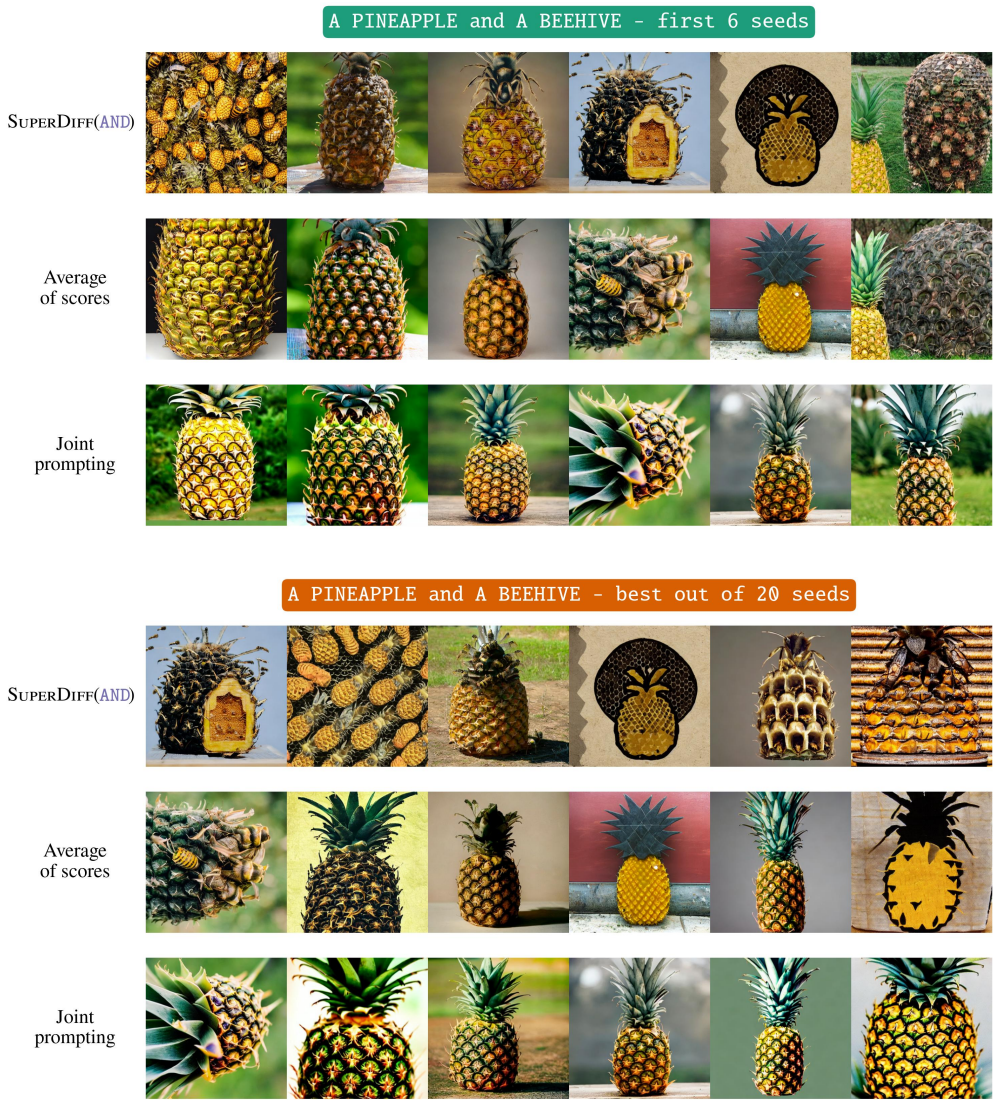

Figure A14: Image compositions generated using SuperDiff (**AND**), averaging of outputs, or joint prompting for the concepts "`a pineapple`" and "`a beehive`".

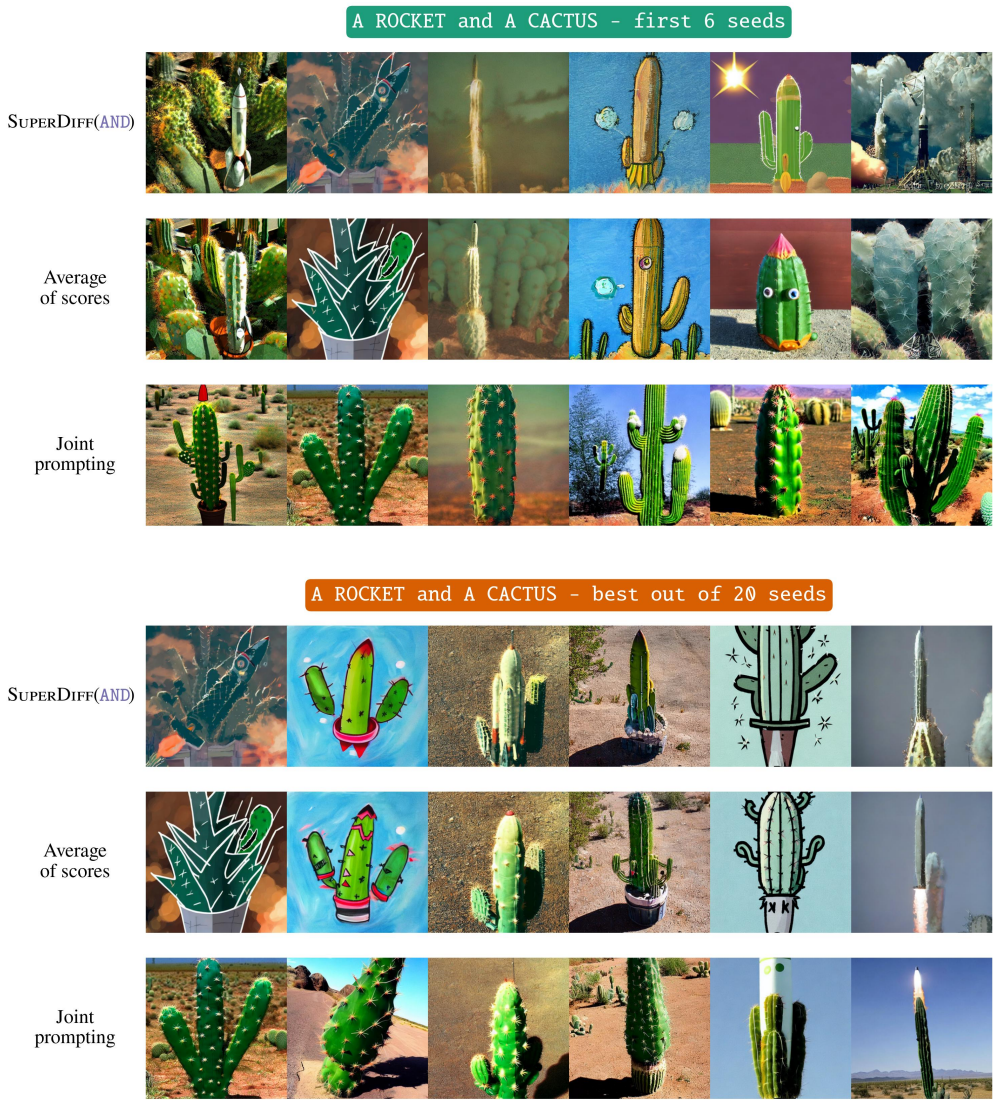

Figure A15: Image compositions generated using SuperDiff (**AND**), averaging of outputs, or joint prompting for the concepts "`a rocket`" and "`a cactus`".

Figure A16: Image compositions generated using SuperDiff (**AND**), averaging of outputs, or joint prompting for the concepts "`a silhouette of a dog`" and "`a mountain landscape`".

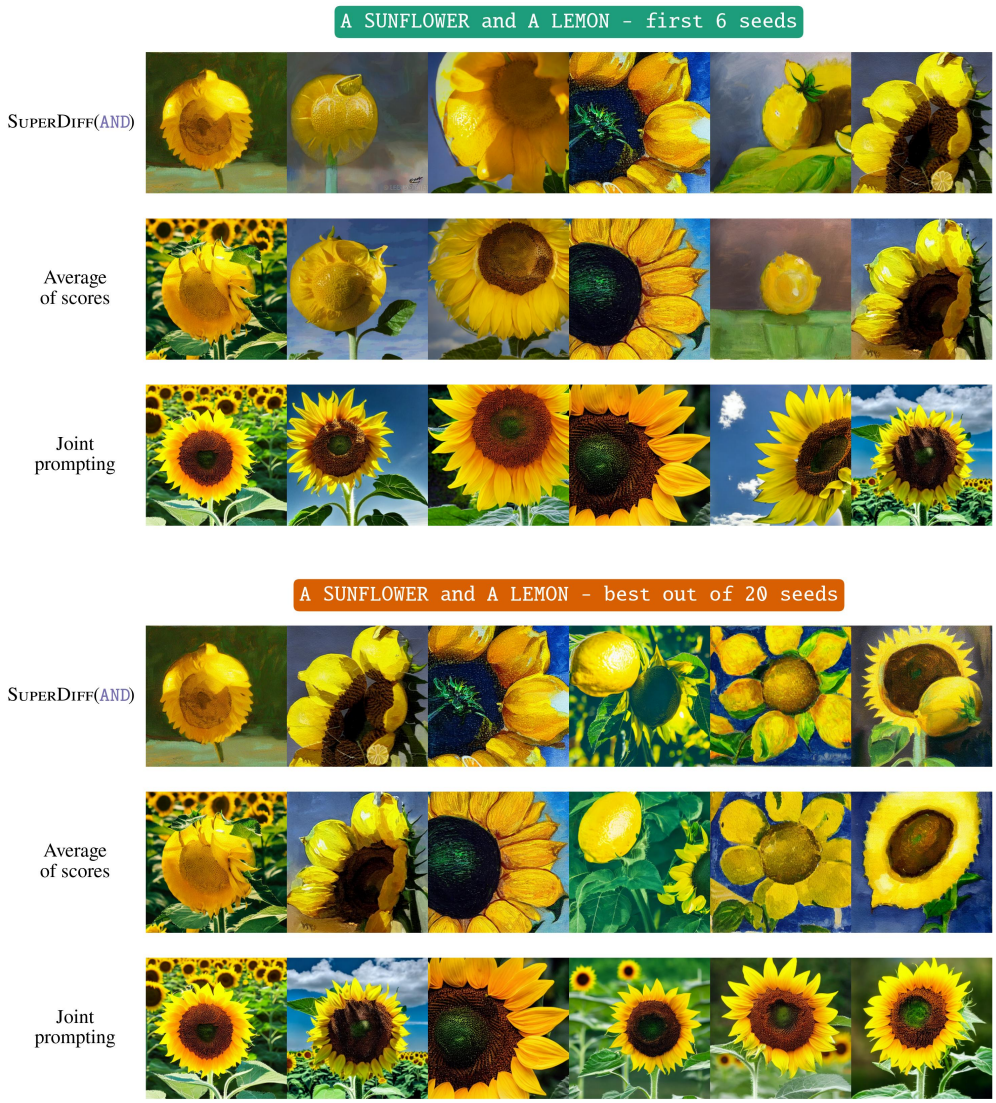

Figure A17: Image compositions generated using SuperDiff (**AND**), averaging of outputs, or joint prompting for the concepts "a sunflower" and "a lemon".

Figure A18: Image compositions generated using SuperDiff (**AND**), averaging of outputs, or joint prompting for the concepts "`teddy bear`" and "`panda`".

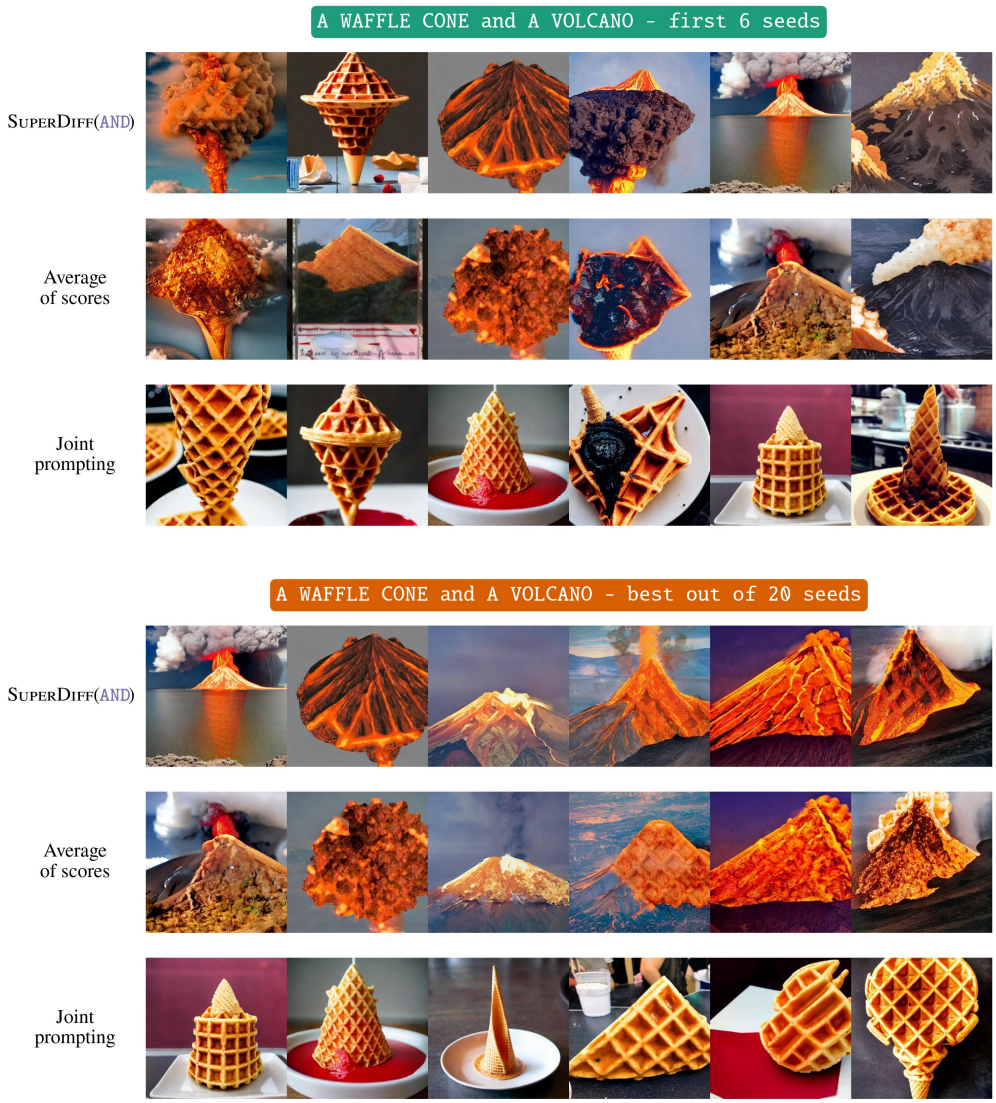

Figure A19: Image compositions generated using SuperDiff (**AND**), averaging of outputs, or joint prompting for the concepts "`a waffle cone`" and "`a volcano`".

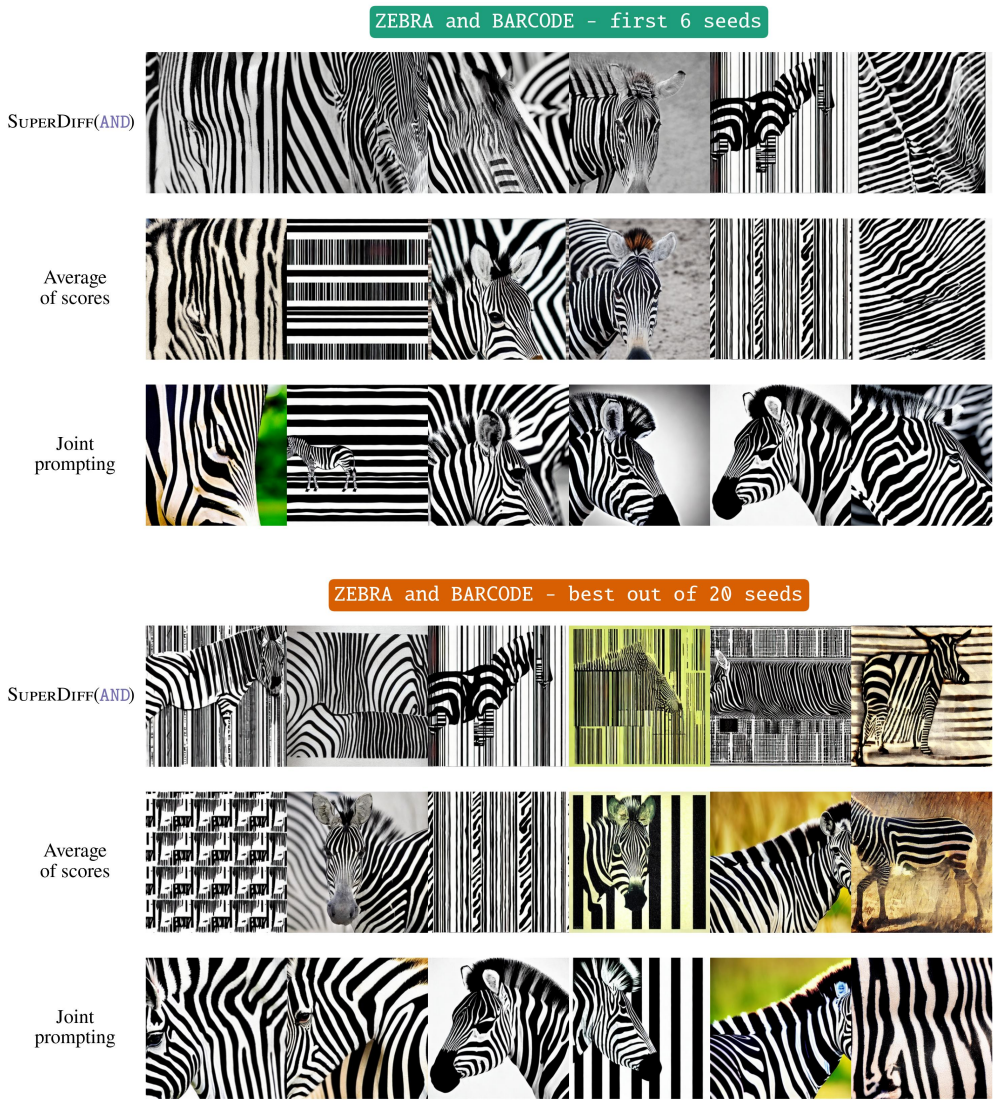

Figure A20: Image compositions generated using SuperDiff (**AND**), averaging of outputs, or joint prompting for the concepts "zebra" and "barcode".

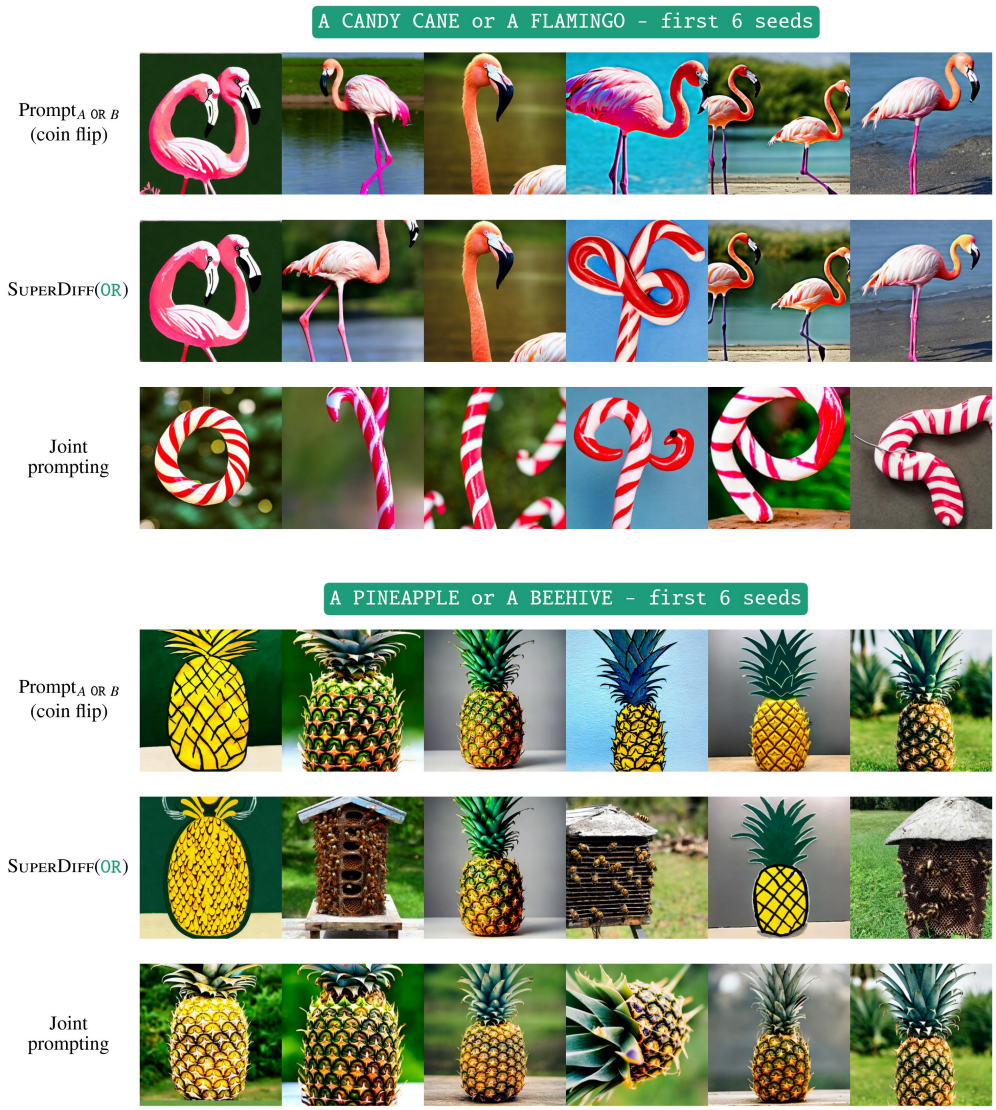

Figure A21: Concept selections using SuperDiff (**OR**), joint prompting, and randomly selecting a prompt of one concept. The top subfigure shows generated images for the concepts `"a candy cane"` or `"a flamingo"`. The bottom subfigure shows generated images for the concepts `"a pineapple"` or `"a beehive"`.